Photocatalytic degradation of RhB dye using hybrid nanocomposite BiOCl@Kaol under sunlight irradiation

Hamza Ighnih, Redouane Haounati, Rahime Eshaghi Malekshah, Hassan Ouachtak, Amane Jada, Abdelaziz Ait Addi

Photocatalytic degradation of RhB dye using hybrid nanocomposite BiOCl@Kaol under sunlight irradiation

*Corresponding authors:

a.aitaddi@uiz.ac.ma ; amane.jada@uha.fr ; ouachtakhassan@gmail.com ; hamza.ighnih@edu.uiz.ac.ma

Graphical abstract

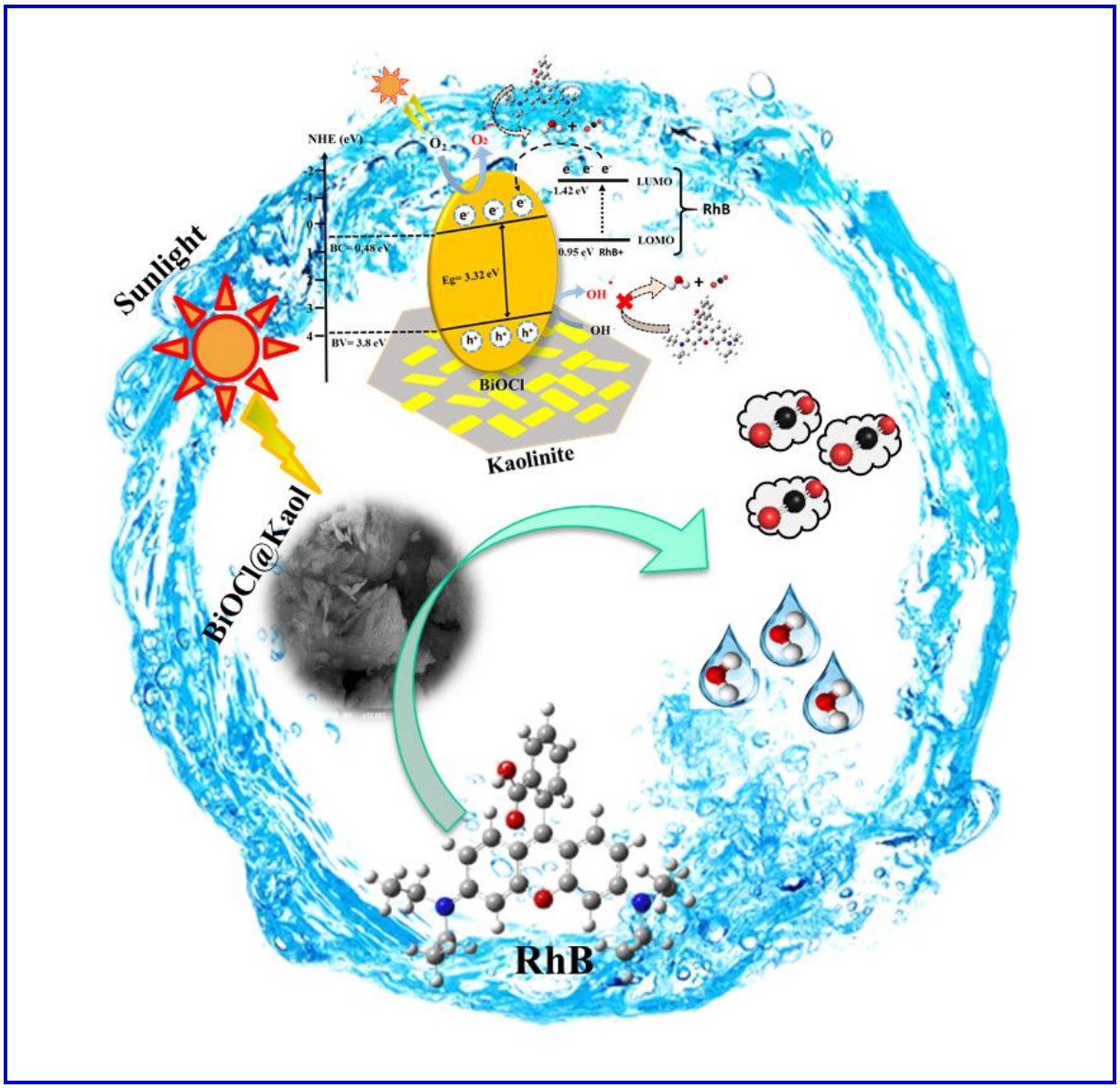

Abstract

The development of advanced photocatalytic materials for environmental purposes is among the hot research topics. In the present work, nanocomposite BiOCl@Kaol, made of kaolinite supported Bismuth Oxy Chloride "BiOCl" photocatalyst, was designed for Rhodamine B dye photodegradation in water. The structures of the BiOCl, as obtained by co-precipitation method, and the clay supported photocatalyst were determined by using various characterization methods, such as X-ray Diffraction (XRD), Fourier Transform Infrared Spectroscopy (FTIR), Scanning Electron Microscopy (SEM), Energy Dispersive Spectroscopy (EDS), Transmission Electron Microscopy and UV-Vis Diffuse Reflectance Spectra. The obtained BiOCl@Kaol nanocomposite was found to have high photocatalytic activity for the removal of Rhodamine B dye (RhB) from water, with a degradation efficiency reaching 100% within 35 minutes. Furthermore, it was observed that the nanocomposite photocatalyst, BiOCl@0.4Kaol, at optimal clay/BiOCl ratio of 0.4, exhibits 4.37 times better photocatalytic performance, in comparison to the bare BiOCl. The scavenger's tests have shown that the superoxide radical is the main species responsible of the RhB dye degradation in water. In addition, the degradation efficiency of RhB by using BiOCl@Kaol nanocomposites was stable after 5 cycles. The overall data indicated that the prepared BiOCl@0.4Kaol photocatalyst has good potential for industrial applications, mainly in the environmental and the energy sectors. Finally, in order to elucidate the photodegradation mechanisms, we have determined various interactions occurring between BiOCl and kaolinite particles, and between RhB molecules and BiOCl@Kaol nanocomposites, by using Monte Carlo calculations. It was concluded from Monte Carlo calculations that hydrogen bonds were established between O atoms of BiOCl and H of kaolinte (001) hydroxyl groups, upon the adsorption of BiOCl (003) particles on the kaolinte (001) surface owing to its high negative interaction energy. Meanwhile, van der Waals attraction was also established between the RhB molecules and the BiOCl@Kaol (001) surface.

Keywords: BiOCl, Kaolinite, Co-precipitation, Photocatalysis, Rhodamine B, Sunlight.

1. Introduction

Nowadays, synthetics dyes are considered among the most hazardous organic pollutants, owing to their complex structures, their stability in aqueous medium, and their highly toxicity[1–3]. In addition, the environmental pollution due to these organic substances is growing continuously leading to various negative impacts [4]. Rhodamine B (RhB) is a dye that is considered potentially toxic due to its ability to cause various health problems [5]. Exposure to high levels of RhB can lead to respiratory tract disorders, gastrointestinal disorders, skin irritation, eye damage [6]. Further its presence in aquatic medium slows down the photosynthesis process [7]. Thus, the removal of RhB dye from aquatic system has a high priority attracted the attention of many researchers due to its impact on health and the environment [8]. Several techniques, such as biological treatment [9], physical adsorption [3,10,11], membrane filtration [12], or chemical oxidation [13], have been explored to remove of RhB dye from aqueous media. Therefore, all these techniques still have many drawbacks, which limits their application, particularly: processing time, low removal efficiency, and high costs. However, It is therefore necessary to explore other sustainable and eco-friendly techniques to remove the RhB dye from aqueous medium [14]. Hence, the advanced oxidation processes (AOP), mainly the photocatalysis technology, is mostly efficient, green, cost effective, widely applied for energy conversion, resulting in green hydrogen production and fast mineralization. The principle of the heterogeneous photocatalysis process is based on the semi-conductor materials (photocatalyst) activation, by using either an artificial or natural (sunlight) radiation source, generating electron-hole pairs which cause various redox reaction at the photocatalyst surface and lead to powerful production of radicals ($HO^{\bullet}$, $O_2^{\bullet-}$, $HO_2^{\bullet}$). The latter are responsible for the degradation of the pollutant molecules and their conversion into H_2O and CO_2.
Recently, several studies have synthesized actives semiconductors for photodegradation of RhB dye in aqueous solution, such as Ag_3PO_4 [15], ZnO [16], TiO_2 [17], $SrHPO_4$ [18], g-C_3N_4 [19]. Whereas, these photocatalysts have many drawbacks which limit their uses, such as, high costly, recombination of electron and hole, lower efficiency, and their difficult regeneration. Over the past few decades, BiOCl photocatalysts have gained attention due to their stability, non-toxic, corrosion resistance, remarkable structure (**Figure 1(a)**), good photocatalytic performance, as well as their low band gap making them suitable for many applications [20–23]. However, pure BiOCl photocatalysts have some disadvantages, including their tendency to form agglomerates in solution, which can reduce their photocatalytic performance. Additionally, the low photo-generated charge separation efficiency can lead to poor photocatalytic activity, high treatment time, and low photocatalytic power under sunlight. However, many researchers have attempted to solve these problems and they proposed heterojunctions establishment of pure BiOCl with other semiconductors photocatalysts such as Cu_2O/BiOCl [24], BiOCl/AgBr [25], BiOCl/g-C_3N_4 [26],

$BiOCl/WO_3$ [27]. Such proposed solutions have disadvantages related to the material cost and its non suitability for its use under sunlight. Therefore, in the present work, one potential solution to improve the photocatalytic properties of BiOCl under sunlight irradiation is to use clay minerals as a support. Clay minerals were selected due to their high specific surface areas, high thermal stabilities, and their low cost, which can help to improve the photocatalytic activity of BiOCl under sunlight. Additionally, clay minerals can also help to prevent the agglomeration of BiOCl and can improve the photo-generated charge separation efficiency, thus leading to enhanced photocatalytic performance. The combination of BiOCl and clay minerals can lead to a photocatalyst having improved stability, higher photocatalytic activity, and better efficiency under sunlight irradiation [28,29]. Various clay mineral types, such as sepiolite [30], palygorskite [31], and zeolite [32] can be used to prevent semiconductors agglomeration. Another type of clay can be used to improve the photocatalytic performance is kaolinite; this clay is very abundant, chemically stable, has large surface area, it is non-toxic, and it has a best catalytic performance [29,33]. Kaolinite is crystallized in the triclinic system with a Tetrahedron silica - Octahedrons alumina (1:1) layer structure (**Figure 1(b, c)**) [34]. Several studies have mostly used kaolinite clay mineral to solve the photocatalysts agglomeration problem as it was observed in systems, such as, TiO_2/kaolinite [35] and g-C_3N_4/kaolinite [36].

In the present work, natural kaolinite was used as support for the BiOCl in order to improve the photocatalyst performance, under sunlight irradiation, and to prevent the hole-electron pairs photo-charged recombination. Therefore, the BiOCl@Kaol nanocomposite was synthetized by Co-precipitation method in acidic medium. Then it was characterized by various methods such as, X-ray diffraction (XRD) to study its structures, Scanning Electron Microscopy (SEM) to observe its topography, Transmission electron microscopy (TEM) to visualize its morphologies and nanostructures, Fourier-transform infrared spectroscopy (FT-IR) to determine its functional groups, and Ultraviolet–Visible Diffuse Reflectance Spectroscopy (UV–Vis DRS) to study its optical properties. The characterized BiOCl@Kaol nanocomposite was thereafter used for rapid removal of RhB dye from aqueous solution, under sunlight irradiation. The adsorption geometries, energetics and electron structural properties of compounds were assessed by DFT-D and MD calculations.

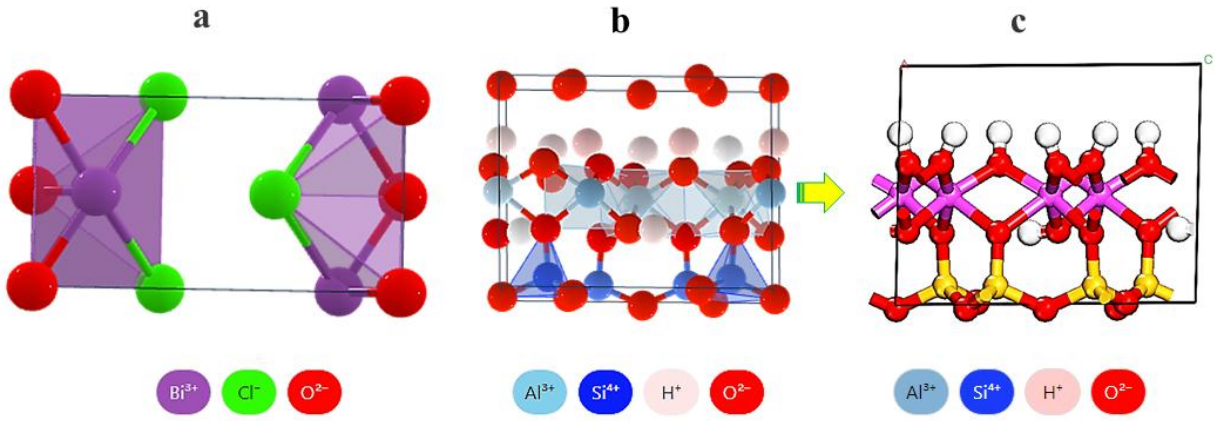

Fig. 1: (a) The unit cell structures of bismuth oxychloride and (b and c) structure of kaolinite.

2. Material and methods

2.1. Photocatalysts preparation

2.1.1. Materials and reagents

Natural kaolinite clay, glacial acetic acid $CH_3CO_2H \geq 99.95\%$), rhodamine B (RhB) dye, bismuth nitrate pentahydrate extra-pure $Bi(NO_3)_3.5H_2O$, sodium chloride ($NaCl \geq 99.5\%$), used in this study were obtained commercially from Sigma Aldrich. All these chemicals reagents were used as received and ~~applied~~ without any purification.

2.1.2. Preparation of BiOCl and BiOCl@Kaolinite

The BiOCl@Kaol was prepared using co-precipitation method in acidic medium. Firstly, 4 mmol of bismuth nitrate pentahydrate was dissolved completely in 40 ml of glacial acetic acid/ deionized water (1:1) solution at 25 °C for 1 hour. Thereafter, 1 g of kaolinite clay was added to the solution under stirring for 1 hour (Solution A). Other solution of sodium chloride was prepared by dissolving 4 mmol of NaCl in 30 mL of deionized water under vigorous stirring for 30 min (solution B). Then, the solution B was slowly added to the solution A under vigorous stirring for 5 h. Finally, the precipitate was filtered, washed three times with distilled water and ethanol, and dried at 70 °C for 12 h and labeled BiOCl@1.0Kaol. By using similar synthesis procedures, BiOCl@Kaol with various mass of kaolinite (0.2, 0.4, 0.6 and 0.8 g) were prepared and labeled as BiOCl@0.2Kaol, BiOCl@0.4Kaol, BiOCl@0.6Kaol, and BiOCl@0.8Kaol, respectively. We followed the same experimental protocol to prepare BiOCl without adding kaolinite. **Figure 2** summarizes the synthesis steps used to prepare the various samples used in the present work.

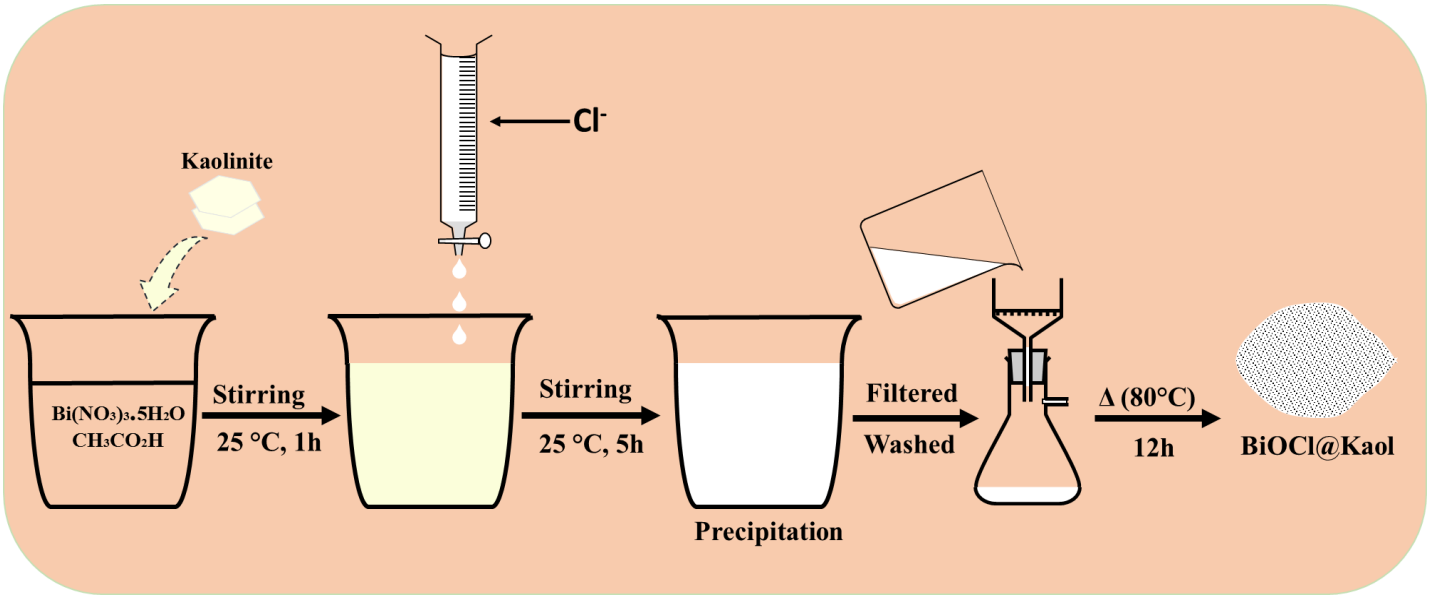

Fig.2: The synthesis steps of BiOCl@Kaol

2.2. Samples characterization

The phase, crystallinity and purity of as-prepared photocatalysts and clay mineral were investigated by X-Ray diffraction technique (Bruker D8 Twin) using monochromatic λ(KαCu) = 1.5418 Å radiation at a step size of 0.05° and scan rate of 1 s/step. The functional groups as determined in the wavenumber region from 400 cm^{-1} to 4000 cm^{-1}, were assessed by using Fourier Transform Infrared Spectroscopy (FTIR). The morphology and microstructure were analyzed by Scanning electron microscopy (Supra 40 VP Gemini Zeiss Column, with a maximum voltage of 20 KV), and the elemental compositions of the composite was performed by recording their Energy Dispersive X-ray (EDX) spectra. The fine structures of the as-prepared photocatalysts were visualized by transmission electron microscopy (TEM). The band gap of all samples was measured using a UV-Vis diffuse reflectance spectra recorded on an UV-Vis Perkin-Elmer Lambda 9.

2.3. Photocatalysis process

The efficiencies of RhB photodegradation in aqueous solution, by using the various prepared samples were studied under solar irradiation. Hence, in a beaker, an amount of 100 ml of RhB dye (10 mg/L) was mixed with 100 mg of the photocatalyst. Prior to the photocatalytic reaction, under sunlight irradiation, an adsorption-desorption equilibrium in the dark for one hour was carried out. During the photocatalytic reaction, 4 mL of the solution was withdrawn each 5 min and then centrifuged. Concentration of residual RhB dye was measured using a UV spectrometer (UV–1800, SHIMADZU), at the wavelength λ=554 nm. The degradation efficiency (DE %) and the rate constants K (min^{-1}) are calculated using **Equations 1 and 2**, respectively**:**

$$DE\% = \frac{C_0 - C_t}{C_0} \times 100 \qquad \textbf{(Eq. 1)}$$

$$Ln\left(\frac{C_0}{C_t}\right) = K \times t \qquad \textbf{(Eq. 2)}$$

Herein, C_0 and C_t are the concentrations of the RhB dye at the initial and any time during photodegradation process, respectively. K (min^{-1}) is the constant of the first-order reaction.

2.4. Calculation methods

2.4.1. Model Construction

Kaolinite (Kaol) as the alternate layers of tetrahedral SiO_4 and octahedral AlO_6 periodically as exhibited in **Figures 3 a** and **b**. $Al_2Si_2H_4O_9$ (code; mp-695878) with Space Group; P1, *a* =5.21, *b* =7.48, *c* = 9.05 Å, α=91.79, β =89.73 γ = 104.97 ° and Volume= 340.74 $Å^3$ was downloaded from https://materialsproject.org/materials/mp-695878. Then, Kaol (001) was constructed based on (001) surface and thickness of 2.06 Å (**Figures 3 c** and **d**) as well as set u v; 2 1, vacuum thickness (0.000) and slab position (1.00). **Figures 3 e** and **(f)** are exhibited Kaol without unit cell. BiOCl including (code; mp-22939) with Space Group; P4/nmm, *a*=*b*= 3.89, c= 7.49 Å, α= β = γ= 90.000° and Volume=113.59 $Å^3$ (**Figure 3g**) was downloaded from https://materialsproject.org/materials/mp-22939. BiOCl (003) was built based on (003) surface and thickness of 3.654 Å as well as set u v; 2 2, vacuum thickness (0.000) and slab position (1.00) (**Figure 3 h**). **Figure 3k** is exhibited BiOCl without unit cell. RhB was built in Material Studio 2017 [37].

2.4.2. Computational method

Kaol, BiOCl and RhB were optimized based DFT-D by $DMol^3$, the generalized gradient approximation (GGA) developed by Perdew-Burke-Ernzerhof (PBE). To locate the optimal adsorption sites of the BiOCl model on two sides of Kaol surface (001), and RhB molecules on two sides of BiOCl@Kaol surface (001), Monte Carlo simulations were used to calculate and performed with universal force field [38]. Two sides of Kaol were studied including HO–Al-terminated (001) surface and Si-terminated (001) surface. The number of cycles was 10, the van der Waals and electrostatic interactions were calculated under the Group -based option at a cutoff of 12.5 Å [39].

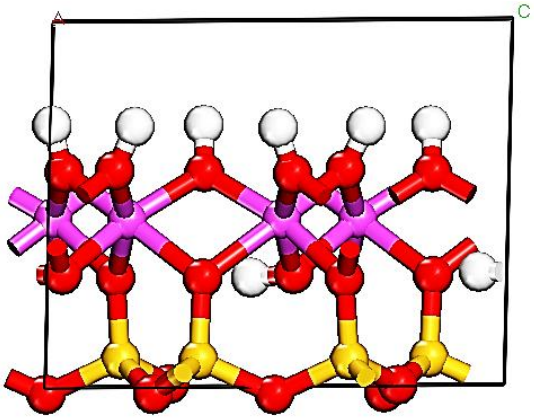

a

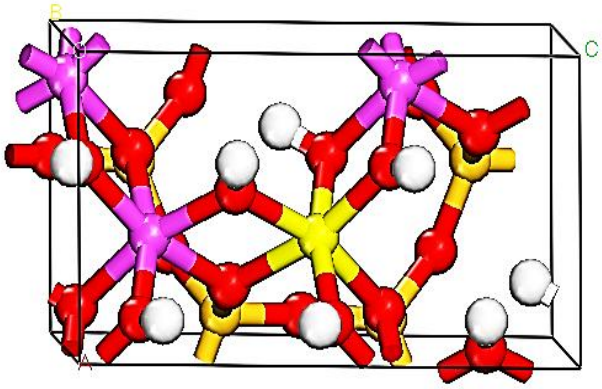

b

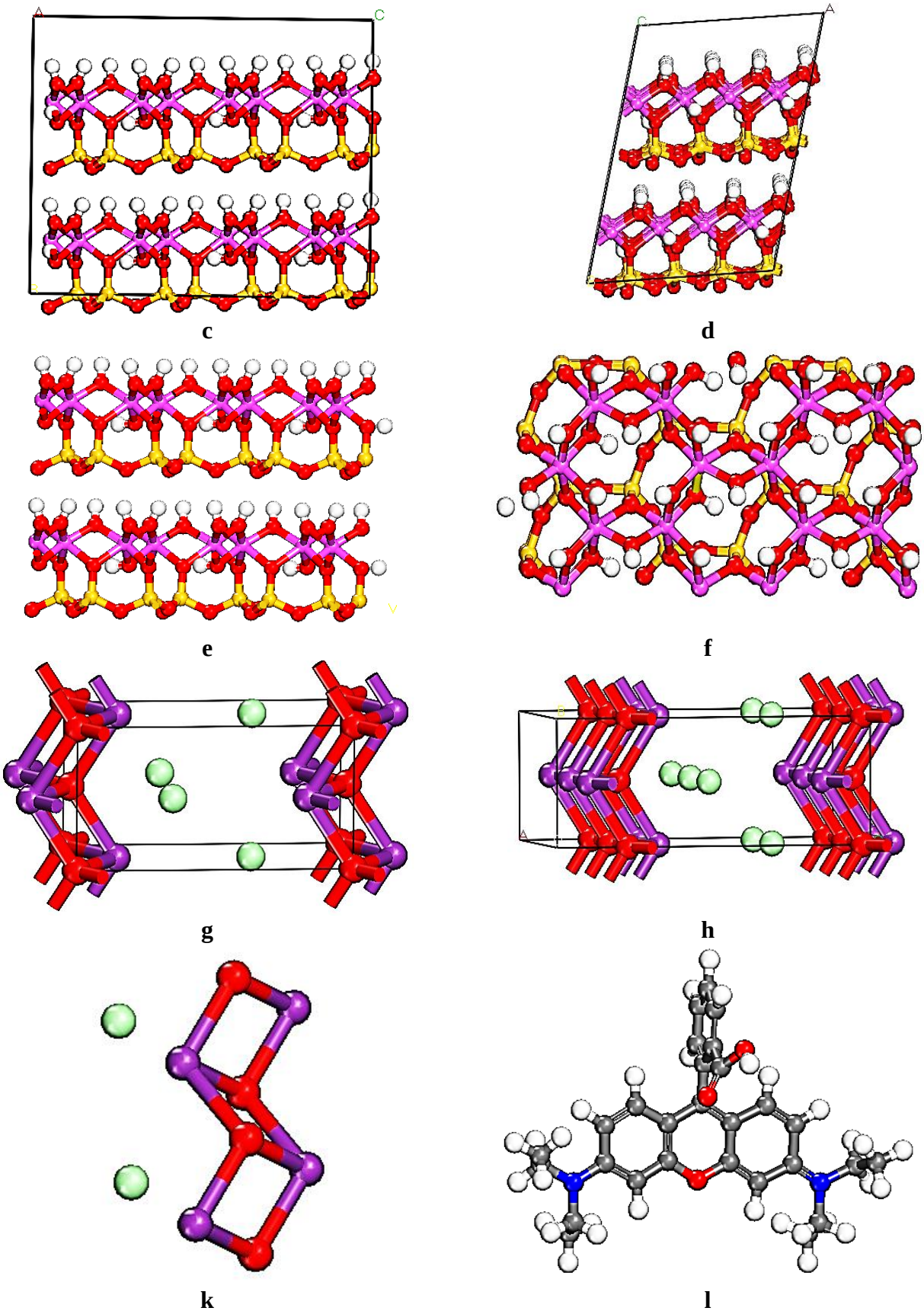

Figure 3. Snapshots of the proposed structures: a (top) and b (side); $Al_2Si_2H_4O_9$ (Kaol), c (top) and d (side) views of Kaol unit cell (001, UV; 2 1), e (top) and f (side) views of Kaol without unit cell (001) (g); BiOCl unit cell (BOC), (g and h); BiOCl unit cell (003, and UV; 2 2), (k); BiOCl without unit cell (003) and (l); RhB. (Yellow ball=Si, purple ball=Al, blue ball= N, grey = C, violet = Bi, green = Cl, red ball=O and white ball=H

3. Results and discussion

3.1. XRD analysis

The X-Ray Diffraction (XRD) patterns of the kaolinite, the as-synthesized BiOCl, and the BiOCl@Kaol, are presented in **Figure 4.** Thus, the XRD peaks located at 2θ=11.95°; 24.1°; 25.9°; 32.55°; 33.45°; 34.8°, 36.5°; 40.9°; 46.7°; 48.4°; 49.7°; 53.25°; 54.15°; 55.05°; 58.65°; 60.65°; and 68.15° were attributed to, respectively, (001), (002), (101), (110), (102), (111), (003), (112), (200), (201), (113), (202), (211), (104), (212), (114), and (220) lattice planes of tetragonal structure of pure BiOCl (JCPDS No. 06-0249). For the kaolinite sample, the XRD peaks located at 2θ= 12.35°; 20.35°; 24.85°; 26.6°; 37.7°; and 62.25° were assigned, respectively, to the planes (001), (110), (002), (003), and (031) according to the card (JCPDS No. 96-900-9235). As expected, the XRD pattern of the serial BiOCl@Kaol composites, exhibited the both the diffraction peaks of BiOCl and kaolinite, showing that BiOCl photocatalysts have been well supported on the kaolinite surface. In addition, the kaolinite (001) and (002) peaks are clearly observed in the XRD diagram of BiOCl@Kaol. These X-ray data shown in Figure 4, confirm that BiOCl@Kaol samples were successfully prepared. It is interesting to note that the intensities of the peaks of kaolinite located at 2θ=12.35° and 2θ=24.85° increase with increasing of the kaolinite/BiOCl weight ratio from 0.2 to 1.0. Such finding can be explained by the increase in kaolinite mass in the BiOCl@Kaol sample. Furthermore, it should be noted that the intensity of BiOCl (001) peak is slightly increased with the increase of the kaolinite/BiOCl weight ratio from 0.2 to 1.0, suggesting that the BiOCl is properly supported on the kaolinite surfaces [38]. The intensities of the (001) and (002) peaks of the kaolinite are strongly reduced in all samples, indicating that the kaolinite clay is well retained by BiOCl nanosheets [26]. In addition, the intensities of the kaolinite peaks (001) and (002), and BiOCl peaks increase when increasing the kaolinite/BiOCl weight ratio from 0.2 to 1.0, this due to the increase in the amount of kaolinite, and the BiOCl crystallinity is increased when moving the kaolinite/BiOCl weight ratio from 0.2 to 1.0 [39,40].

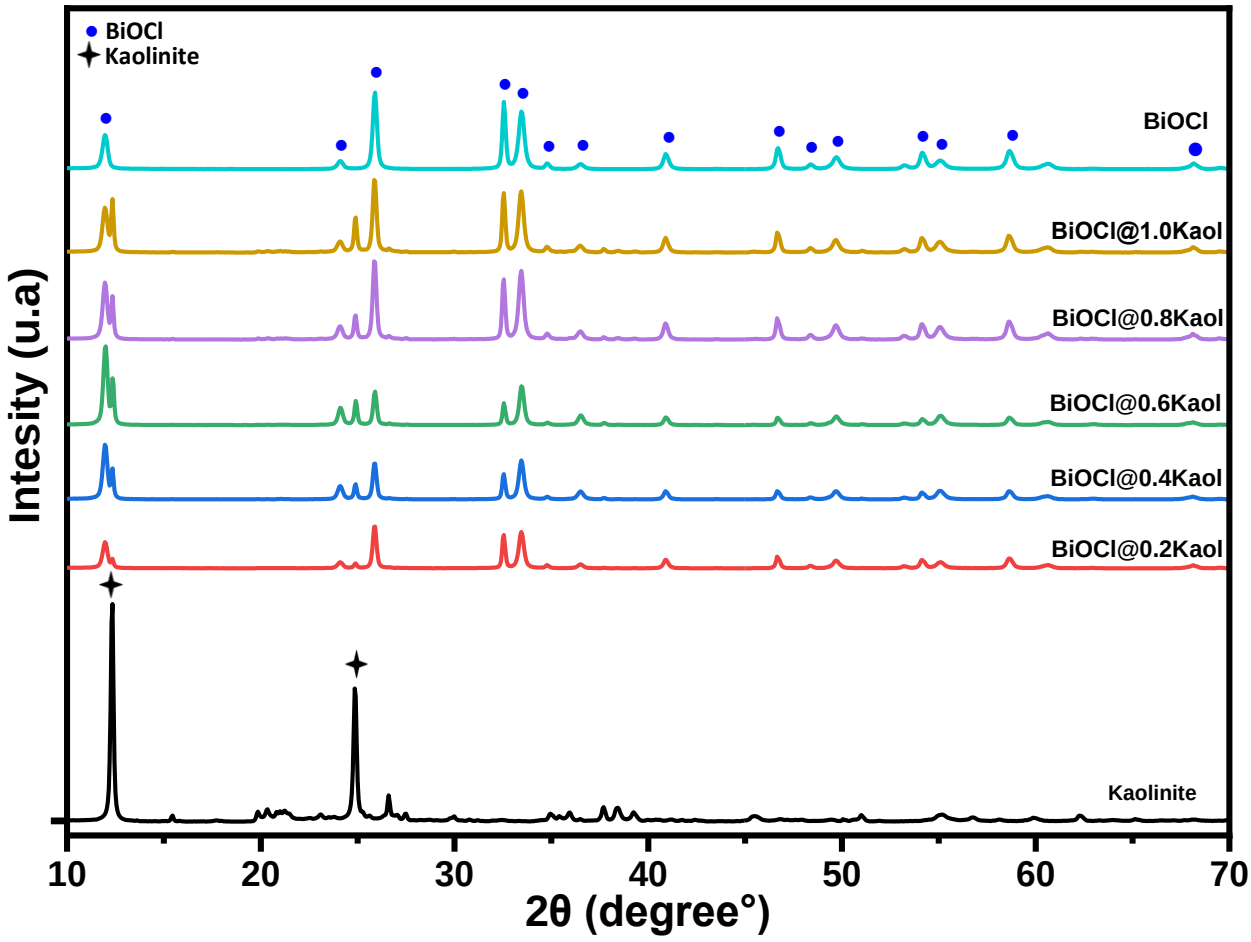

Fig. 4: XRD of all prepared samples

3.2. FTIR analysis results

Figure 5. shows the spectra obtained from FTIR analysis of all prepared samples. The FTIR spectrum of raw kaolinite, as presented by the black line in this figure, shows the presence of two characteristics bands at 428.19 cm^{-1} and 1006.84 cm^{-1}, attributed to the stretching vibration of Si–O. The characteristic bands located at 468.70 cm^{-1} and 1029.98 cm^{-1} are attributed the deformation modes of Si-O-Si group. The band at 536 cm^{-1} is attributed to Al-O-Si deformation of the kaolinite. Furthermore, the characteristics bands at 3618.45 cm^{-1} and 3697.54 cm^{-1} correspond to the OH stretching of the Al–OH and Si–OH groups, respectively [31]. On the other hand, the FT-IR spectrum of pure BiOCl displays a band located at about 529.37 cm^{-1} which is attributed to the stretching vibrations of Bi-O [30]. The characteristic band with low intensity, and located at 1635 cm^{-1} can be associated to the stretching vibration mode of Bi-Cl. The overall FT-IR spectra of all photocatalysis samples show characteristics bands of both the kaolinite clay and the pure BiOCl, with a slight increase of intensity of kaolinite band when its mass increases in the kaolinite/BiOCl weight ratio.

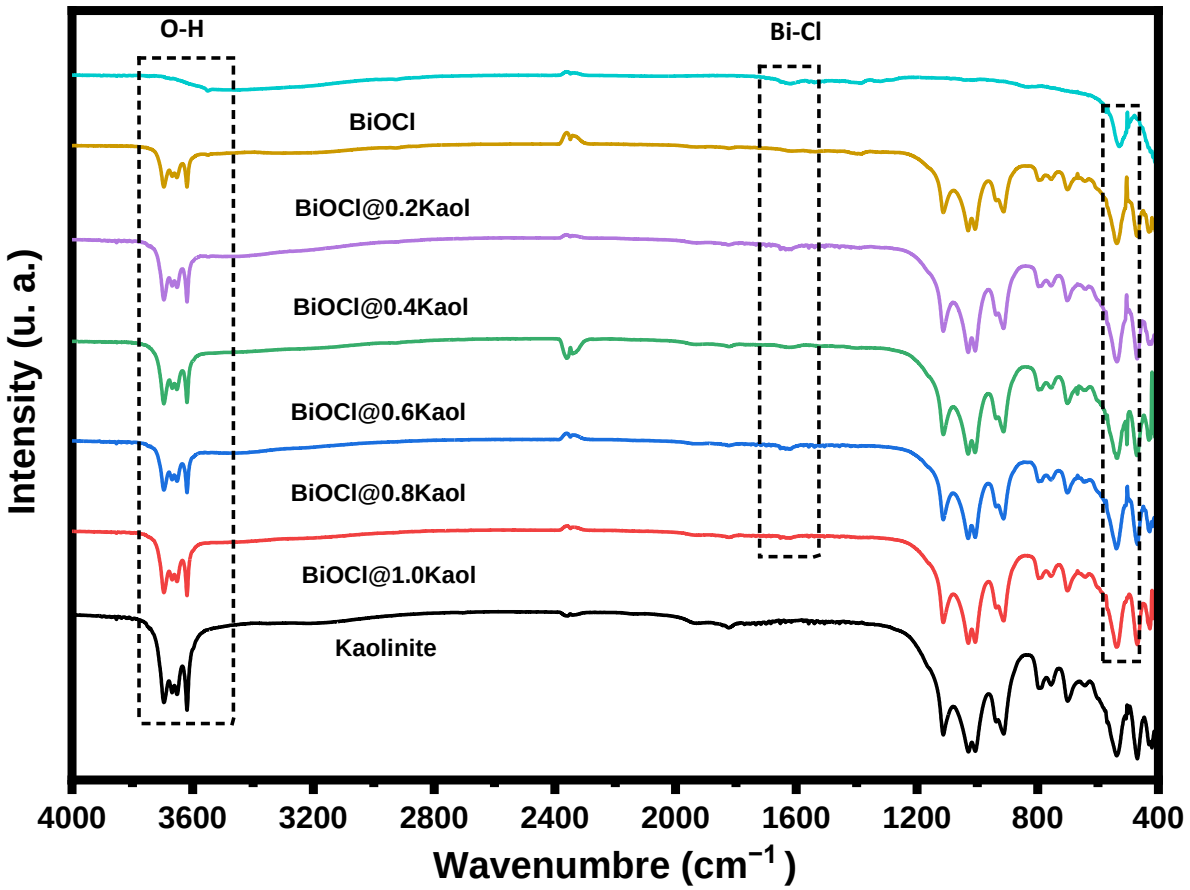

Fig. 5: FT-IR of the as prepared samples.

3.3. SEM analysis results

The morphologies and the elementary compositions of the raw kaolinite, pure BiOCl, and BiOCl@0.4Kaol, are shown in **Figure 6**. The SEM images of the raw kaolinite (**Figure 6** (**a**, **b**)) show that the kaolinite particle consists of tightly packed layered hexagonal morphology, due to the presence of hydrogen interaction occurring between the aluminosilicate sheets.

The SEM images of pure BiOCl particles (Figure 6 (d, e)), exhibit a spherical gathering of many thin nanosheets, resulting in uniform micro flower shape. Moreover, (**Figure 6 (j, h)**), shows the SEM images of BiOCl@0.4Kaol nanocomposite. As can be seen from these images, the nano plates of the BiOCl catalyst are well supported on the kaolinite sheets. In addition, the EDX spectra and mapping of the kaolinite (Figure 6 (c)), the pure BiOCl (Figure 6 (f)), and the BiOCl@0.4Kaol (Figure 6 (i)), indicate that the raw kaolinite mineral contains the expected elements Al, Si and O, and that the pure BiOCl includes the Bi, O, and Cl atoms with an equal molar ratio. For the BiOCl@0.4Kaol, it can be observed that the atoms were evenly distributed throughout the sample, indicating that the BiOCl was evenly dispersed on the kaolinite clay.

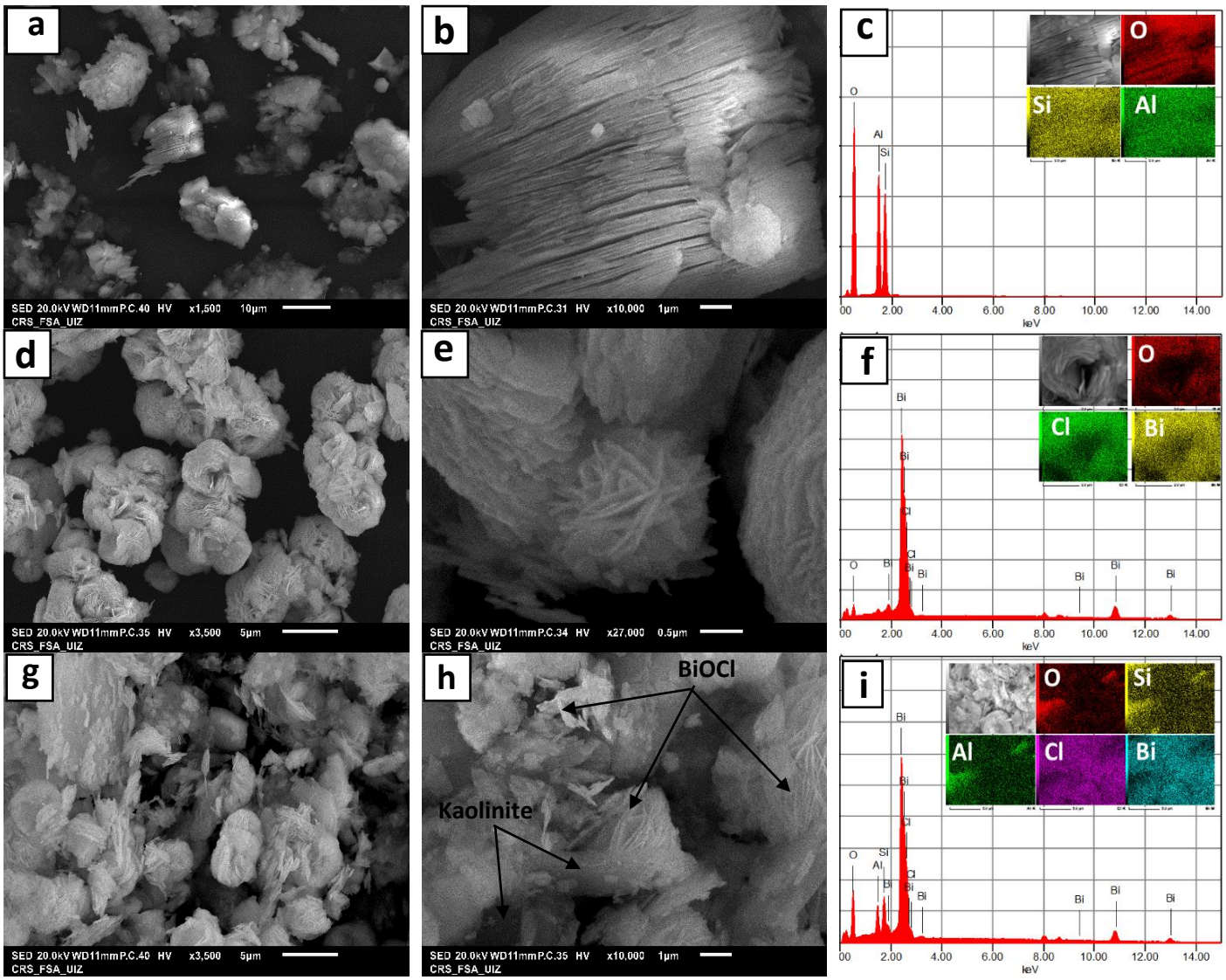

Fig. 6: Typical SEM images and EDX spectra and mapping of (a, b, c) raw kaolinite (d, e, f) pure BiOCl and (g, h, i) of BiOCl@0.4Kaol.

3.4. TEM analysis results

The morphologies and nanostructures of as-synthetized BiOCl@Kaol samples were investigated by Transmittance Electron Microscopy (**Figure 7**). The **Figure 7 (a, b)** displays the TEM images of BiOCl particles, indicating that they consist of two-dimensional nanosheets type, having a diameter size between 80-600 nm with the appearance of metallic Bi nanoparticles. The TEM images of raw kaolinite (**Figure 7 (c, d)**), show two-dimensional nano layered with a diameter size between 0.5 – 1.2 µm. Regarding the BiOCl@Kaol nanocomposite, it can be observed from **Figure 7 (e, f)**, that the BiOCl mirco flowers shaped particles were fixed on the kaolinite surface.

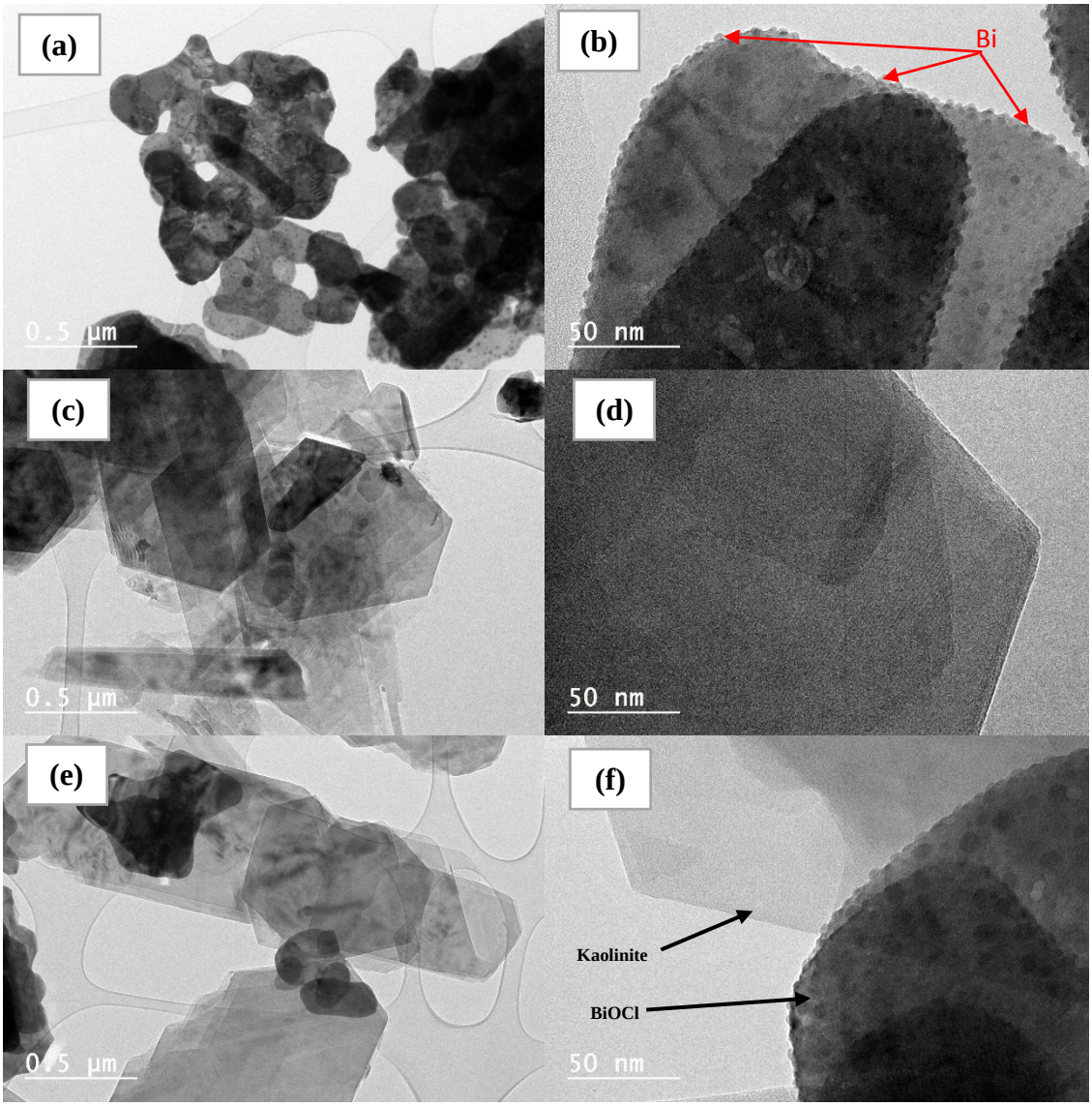

Fig. 7: The high- resolution TEM (HRTEM) images of BiOCl (a, b), kaolinite (c, d) and BiOCl@Kaol nanocomposite (e, f).

3.5. Optical absorption properties and band gap energy of samples

The optical properties of the raw kaolinite, the pure BiOCl, and the different BiOCl@Kaol samples having various kaolinite/BiOCl weight ratios, were studied by UV–vis Diffuse Reflectance Spectra (DRS). The **Figure 8 (a)** illustrate the UV–vis absorption spectrum of as prepared in the range of 200 – 800 nm. It can be observed that the bands edge absorptions of, pure BiOCl, raw kaolinite BiOCl@0.2Kaol, BiOCl@0.4Kaol, BiOCl@0.6Kaol, BiOCl@0.8Kaol, and BiOCl@1.0Kaol are located at 390, 420, 385, 400, 375, 380, and 383 nm, respectively. It should be noted that the observed higher absorption capacity of raw kaolinite in the visible light range, results from the heterogeneous construction of the tetrahedral and the octahedral aluminosilicate sheets [14]. In contrast, the BiOCl@0.4Kaol sample displays the best absorption capacity (band edge absorption of 400 nm) in the visible light, as compared with others samples having various kaolinite/BiOCl

weight ratios, and pure BiOCl. Moreover, the band gap energies of the synthetized catalysts **are** described by the Tauc's equation as follow (**Equation 3**) [32].

$$\alpha h\nu = C(h\nu - E_g)^{n/2} \qquad \textbf{(Eqn. 3)}$$

Where α, hν, C and Eg, are the absorption coefficient, the photon energy, proportional constant, and band gap energy, respectively. The value of n depends on the property of the semiconductor (n=1 or 4 for direct band gap or indirect band gap separately). For a semiconductor with indirect band gap, BiOCl, the value of n is equal 4.

The F**igure 8 (b)** shows the plot of $(\alpha h\nu)^{0.5}$ versus the photon energy. The calculated E_g of as prepared catalysts are presented in **Table 1**. The estimated gap energy value of pure BiOCl and BiOCl@0.4Kaol were about 3.32 and 3.19 eV, respectively. Therefore, the band gap, for the sample having the optimal kaolinite/BiOCl weight ratio of 0.4, is the lowest compared to the others clay/BiOCl weight ratios.

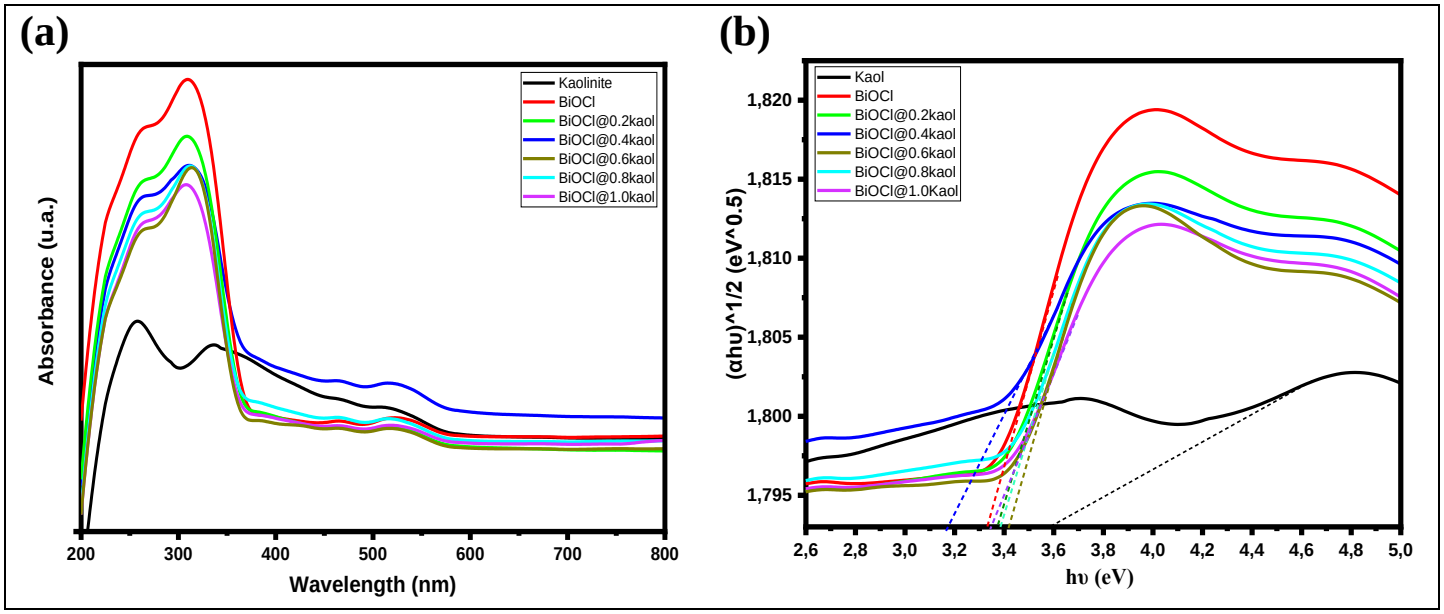

Fig. 8: (a) UV-DRS and (b) Eg of as-prepared samples.

Table 1: Gap energy of the various prepared samples

Photocatalysts	Kaol	BiOCl	BiOCl@0.2Kaol	BiOCl@0.4Kaol	BiOCl@0.6Kaol	BiOCl@0.8Kaol	BiOCl@1.0Kaol
Eg (eV)	3.59	3.32	3.38	3.19	3.39	3.35	3.41

3.6. Photocatalytic degradation of RhB dye

The photocatalytic process of the samples was investigated in RhB solution at room temperature under sunlight irradiation. **Figure 9** shows the adsorption-desorption equilibrium test, photolysis (absence of photocatalyst) and photocatalysis tests. As shown in **Figure 9 (a)**, in the case of photolysis process without photocatalyst, the rate of degradation of RhB dye did not exceed 2%

after 60 min. Consequently, it can be concluded that the photodegradation of RhB dye is not possible using photolysis.

Adsorption tests for all samples show that the highest adsorption efficiency is 44.43% after 60 min, recorded by the BiOCl@0.4Kaol. The results in **Figure 9 (a)** revealed that BiOCl@Kaol composites have good degradation efficiencies as compared to the pure BiOCl. In addition, the BiOCl@0.4Kaol composite presents the highest photocatalytic performance (DE% ≈ 100% in the first 35 minutes of irradiation) compared to the others samples (**Figure 9 (b)**). The lowest degradation efficiency of the pure BiOCl is 71%, is due to the electron–hole recombination and agglomeration phenomena of BiOCl.

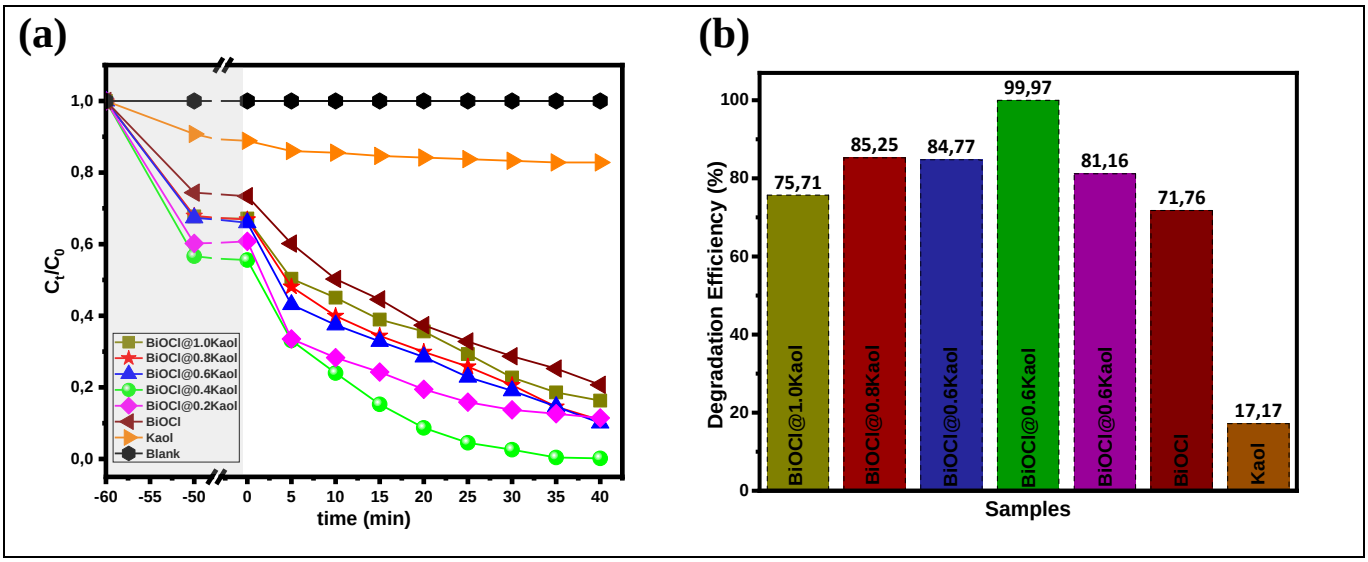

Fig. 9: (a) Adsorption and photocatalytic degradation of RhB dye under sunlight, (b) Degradation efficiency of RhB dye

Therefore, the kinetic of photodegradation of as-prepared BiOCl@0.2Kaol, BiOCl@0.4Kaol, BiOCl@0.6Kaol, BiOCl@0.8Kaol, BiOCl@1.0Kaol, BiOCl, and kaolinite, have been further examined according to the Langmuir-Hinshelwood model using the first-order kinetic formula:

$$Ln\left(\frac{C_0}{C_t}\right) = K \times t \qquad \textbf{(Eqn. 4)}$$

The rate constant K(min^{-1}) is determinate graphically from the slopes of the linear plots (**Figure 10 (a)).** **T**he values of K(min^{-1}) are presented in **Figure 10 (b)**. From these results, all the apparent reaction rate constant K(min−1) values, corresponding to the BiOCl@Kaol composites are superior to those obtained for pure BiOCl ones, and K(BiOCl@0.4Kaol) has a great value (K=0.139 min^{-1}). It is interesting to note that the rate constant for BiOCl@0.4Kaol was 4.37 times that of pure BiOCl (Figure 10 (b)). These results confirmed that the surface and structure of the kaolinite clay play a very important role in improving the rapidity of degradation of RhB dye.

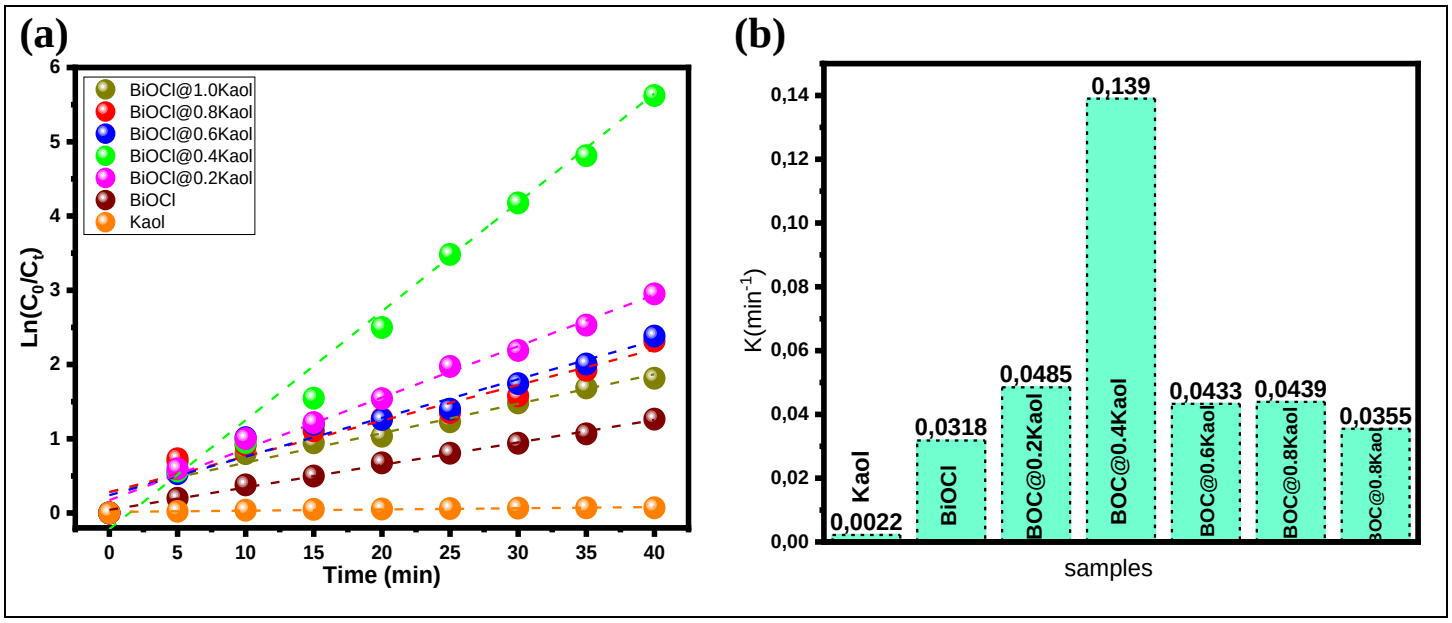

Fig. 10: (a) Photocatalytic kinetic using first-order kinetic (b) The rate constant kinetic values.

3.7. Simulation Methods

3.7.1. Quantum calculations

To obtain optimized structures and energies, the generalized gradient approximation (GGA), using the Perdew-Burke-Ernzerhof (PBE) functional were adopted and the stable configurations are shown in **Figures 11 (a–c)**. Total energy of Kaol, BiOCl and RhB was obtained -27740.463, -1243.137 and -1880.764, Ha, respectively. The geometric parameters of Kaol, BiOCl and RhB are summarized in **Table 2.**

Table 2: The geometric parameters of all compounds obtained by DMol^3 based on DFT-D (Ha).

	Kaol	BiOCl	RhB
Sum of atomic energies	-27686.708	-1241.484	-1868.168
Kinetic	-126.215	0.912	-18.431
Electrostatic	39.296	-3.443	-2.017
Exchange-correlation	20.682	0.329	4.536
Spin polarization	12.481	0.548	3.394
DFT-D correction	-	-	-0.079
Total Energy	-27740.463	-1243.137	-1880.764

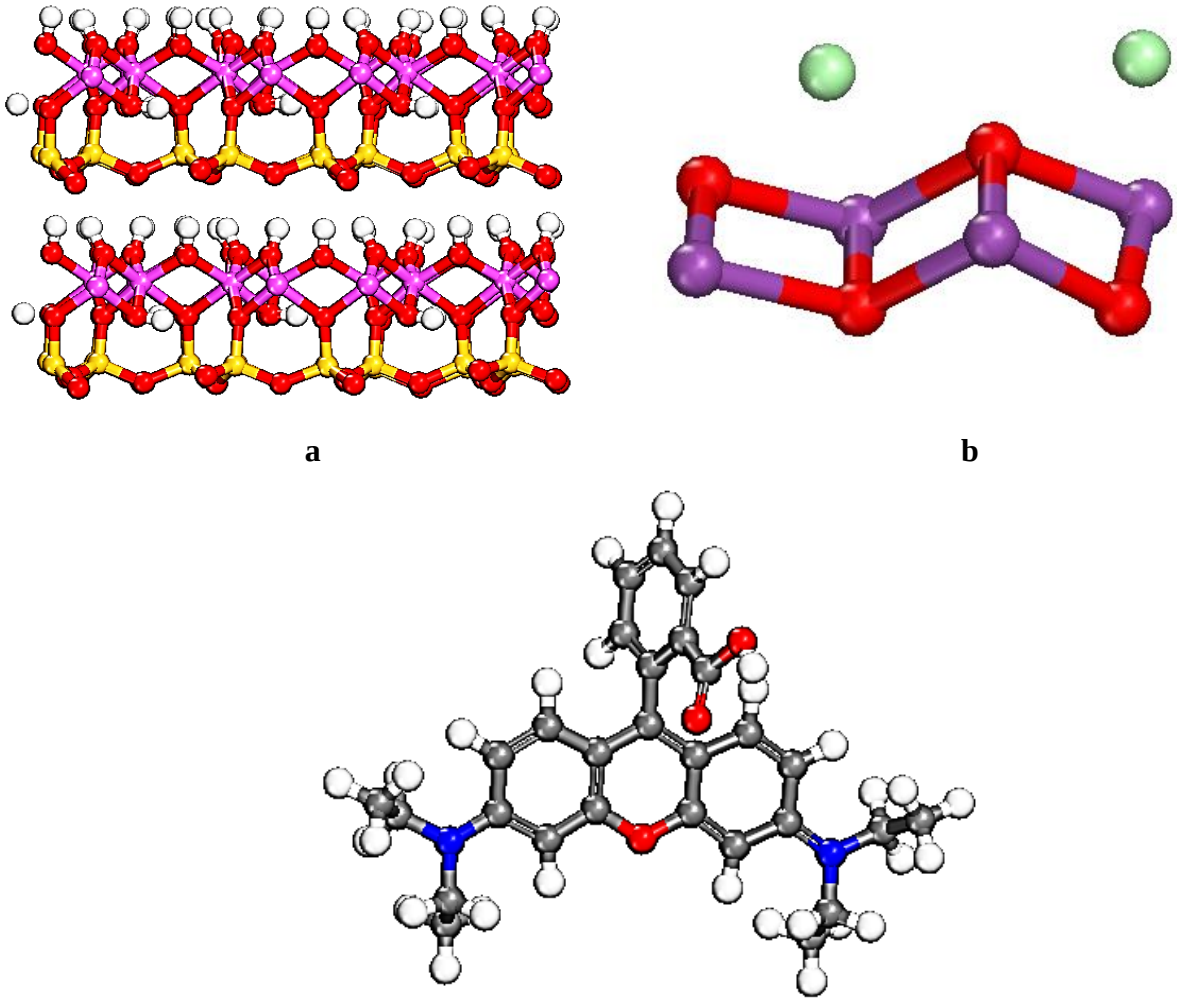

a **b**

c

Fig. 11: The low-energy configuration (a); Kaol (001), (b); BiOCl (003) and (c); RhB obtained from DMol^3 Based on DFT-D.

3.7.2. Modelling by Monte Carlo adsorption locator simulation

After optimization of compounds by quantum calculations, the adsorption of 5 BiOCl (003) molecules on Kaol (001) was investigated to make BiOCl@Kaol by adsorption locator module and force field; universal in Materials Studio 2017 software. The electrostatic and van der Waals was calculated using the Group summation method [40].

The lowest energy structures of BiOCl@Kaol through MD calculations are presented in **Figure 12**. The total energy of the adsorption system for BiOCl@Kaol was obtained about -2.023×10^{3} Kcal/mol, demonstrating the exothermic and stability of the adsorption system owing to its high negative interaction energy. The negatively charged regions were mainly distributed around the O atoms of the lying hydroxyl on kaolinite (001) surface [41]. BiOCl molecules were approximately parallel on OH groups in addition to Si-terminated (001) surface of the kaolinite in the equilibrium configurations. In addition, the kaolinite (001) surface had the ability to form three hydrogen bonds between O atoms of BiOCl and OH groups of Kaol (001) with less than 3 Å (**Figure 13**).

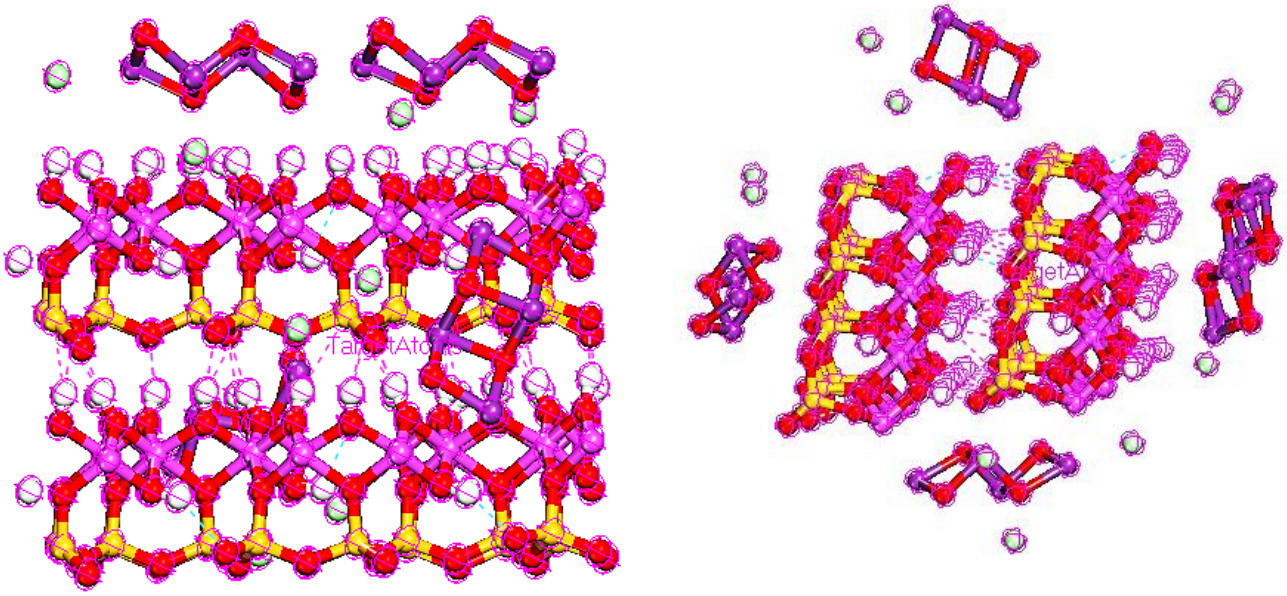

a **b**

Fig. 12: (a); Top and side (b); views of the adsorption of 5 BiOCl (003) molecules on Kaol (001) obtained by adsorption locator module in Materials Studio 2017 software.

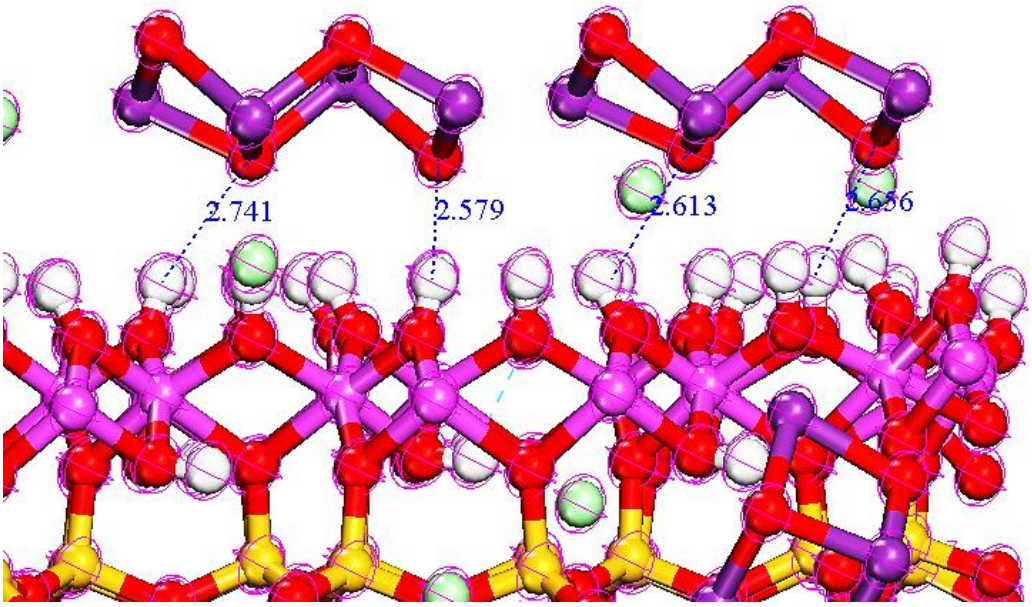

Fig. 13: The hydrogen bonds between O atoms of BiOCl and O atoms of Kaol (001) obtained by adsorption locator module in Materials Studio 2017 software.

In next stage, BiOCl@Kaol adsorbate was prepared to adsorb 6 RhB molecules, by the Monte Carlo adsorption locator module. The adsorption energy (E_{ad}) of RhB on BiOCl@Kaol was evaluated -233.816 Kcal/mol and the adsorption energy of RhB on BiOCl@Kaol was more compared with the adsorption energy of RhB on BiOCl and Kaol. The adsorption energy of the RhB molecules on BiOCl@Kaol surface was negative, suggesting the adsorption strength of RhB molecules. The pollutants were interacted over kaolinite surface of BiOCl@Kaol (**Figure 14**).

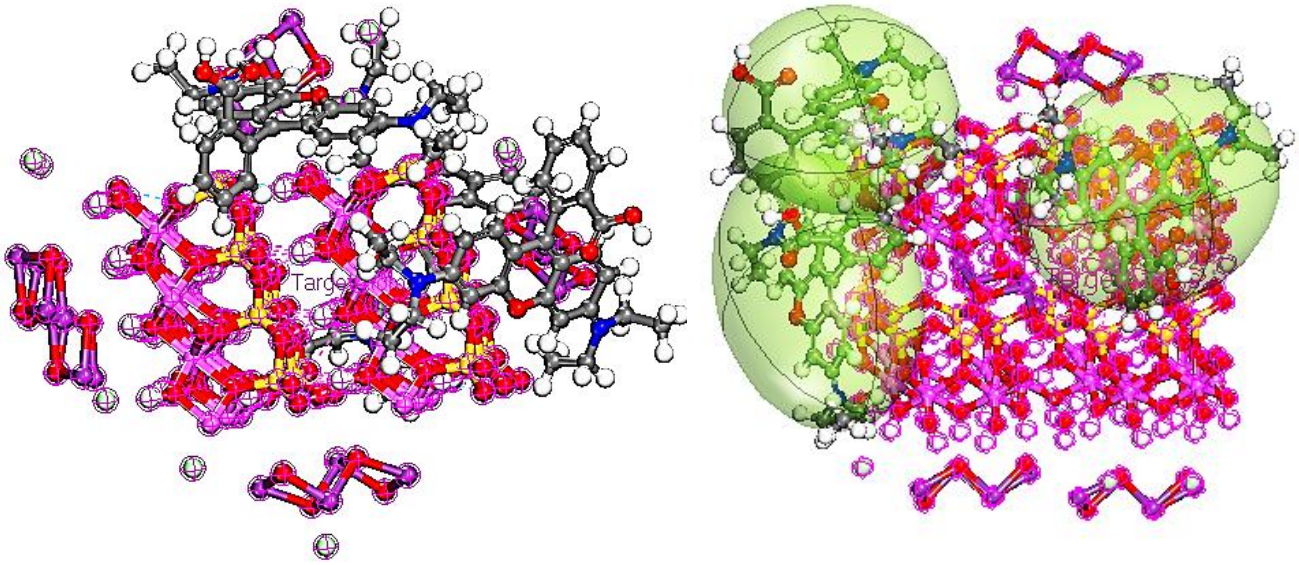

Fig. 14: Configurations of adsorption of RhB on BiOCl@Kaol by adsorption locator module in Materials Studio 2017 software.

3.8. Possible Photocatalytic mechanism

To provide better understanding the photocatalytic mechanism, several species were investigated. The main species responsible for the degradation of organic pollutant are generally hydroxyl radicals (HO•), superoxide radicals (O_2•$^-$), and holes (h^+). Species named scavengers were used to determinate which species radicals responsible on the degradation process. Acid ascorbic (Asc), Isopropanol alcohol (Ipr), and ethylene diamine tetra acetic acid (EDTA), are the most commonly scavengers using to trapping radicals (O_2•$^-$), (HO•), and (h^+), respectively. In our experience, 4 mmol of each scavenger was added in 100 mL of RhB dye solution (10ppm), with 100 mg of BiOCl@0.4Kaol, and agitated under sunlight irradiation for 20 min, after that the solution is separated by centrifuge, and then the concentration of RhB dye is determined using UV-vis spectrophotometry. The obtained experimental results of the three trapping tests were presented in the **Figure 15.** So, the degradation efficiency without any scavengers attain 100% in 35 min. In presence of (Asc), (EDTA) and (iPr), the degradation rate decrease from 100% to 13%, 85%, and 84%, respectively (Figure 15). However, the significant decrease in the presence of ascorbic acid indicate that the superoxide radicals (O2•-) is the main radical species causing the RhB dye photodegradation over BiOCl@Kaol. In addition, the EBV and EBC edge potential of the BiOCl@Kaol semiconductor are calculated using the following empirical formulas (Equations 5–7) [43]:

$$\chi(A_aB_bC_c) = [\chi A^a . \chi B^b . \chi C^c]^{\frac{1}{a+b+c}} \qquad \textbf{(Eqn. 5)}$$

$$E_{BC} = \chi(A_aB_bC_c) - E_0 - \frac{E_g}{2} \qquad \textbf{(Eqn. 6)}$$

$$E_{BV} = E_{BC} + E_g \qquad \textbf{(Eqn. 7)}$$

Where χ (eV) is the absolute electronegativity of the BiOCl semiconductor, and a, b, and c are the number of atoms in a chemical formula $A_aB_bC_c$. E_{VB}, E_{CB}, and Eg are the valence band edge potential, conductor band edge potential, and the band gap energy of semiconductor respectively. E_0 (eV) is the energy of free electrons on the hydrogen scale ($E_0 \approx 4.5$ eV/NHE) [42]. The calculate value of χ(BiOCl), Eg, E_{VB}, and E_{CB} are listed in the **Table 3.**

Based on the experimental results of scavenger's test, which indicating that the main responsible for the degradation is the superoxide **($O_2^{\bullet-}$)**, the O_2 reduction potential (**$E(O_2/O_2^{\bullet-}) = -0.33$ eV**) is more negative than that of E_{CB} (**0.41 eV**). Therefore, it is impossible to reduce **O_2** directly by excitation of BiOCl semiconductor. However, to explain the obtained experimental results, we purpose the following mechanism, RhB dye can be degraded by the transfer to the excited state (RhB*) under

sunlight irradiation (**Eqn. 8**), through the transfer the electrons of RhB molecules on the highest occupied molecular orbital (HOMO), to the lowest unoccupied molecular orbital (LUMO), then the electrons of LUMO edge will be passing to the E_{CB} ($\mathbf{e^-_{CB}}$) of BiOCl **(Eqn. 9),** and react with $\mathbf{O_2}$ for formed superoxide radicals ($\mathbf{O_2^{\bullet-}}$) **(Eqn. 10)** [43,44]. This radical reduces the excited rhodamine B (RhB*) molecular to H_2O and CO_2 (**Eqn. 11**). **Figure 16** present the possible mechanism of the RhB photodegradation reaction by BiOCl@Kaol.

$$RhB + h\upsilon \longrightarrow RhB^* \qquad \textbf{(Eqn. 8)}$$

$$\mathbf{BiOCl@Kaol} + RhB^* \longrightarrow e^-_{CB} + RhB^{\bullet+} \qquad \textbf{(Eqn. 9)}$$

$$e^-_{CB} + O_2 \longrightarrow O_2^{\bullet-} \qquad \textbf{(Eqn. 10)}$$

$$O_2^{\bullet-} + RhB^{\bullet+} \longrightarrow CO_2 + H_2O \qquad \textbf{(Eqn. 11)}$$

Table 3: Obtained values of CB and VB potentials of BiOCl

Parameter	E_0 (eV/NHE)	χ (eV)	Eg (eV)	E_{VB} (eV)	E_{CB} (eV)
Values	4.5	6.64	3.32	3.8	0.48

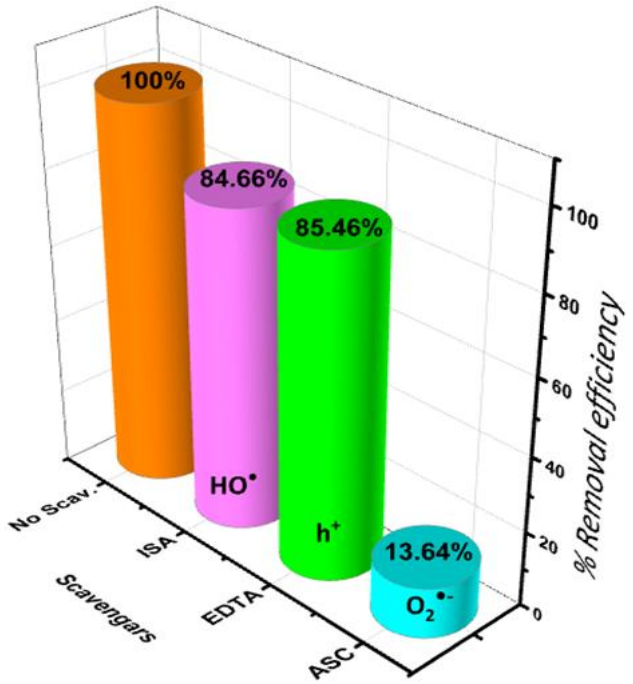

Fig. 15: The species trapping experiments for photodegradation of RhB dye by BiOCl@0.4Kaol.

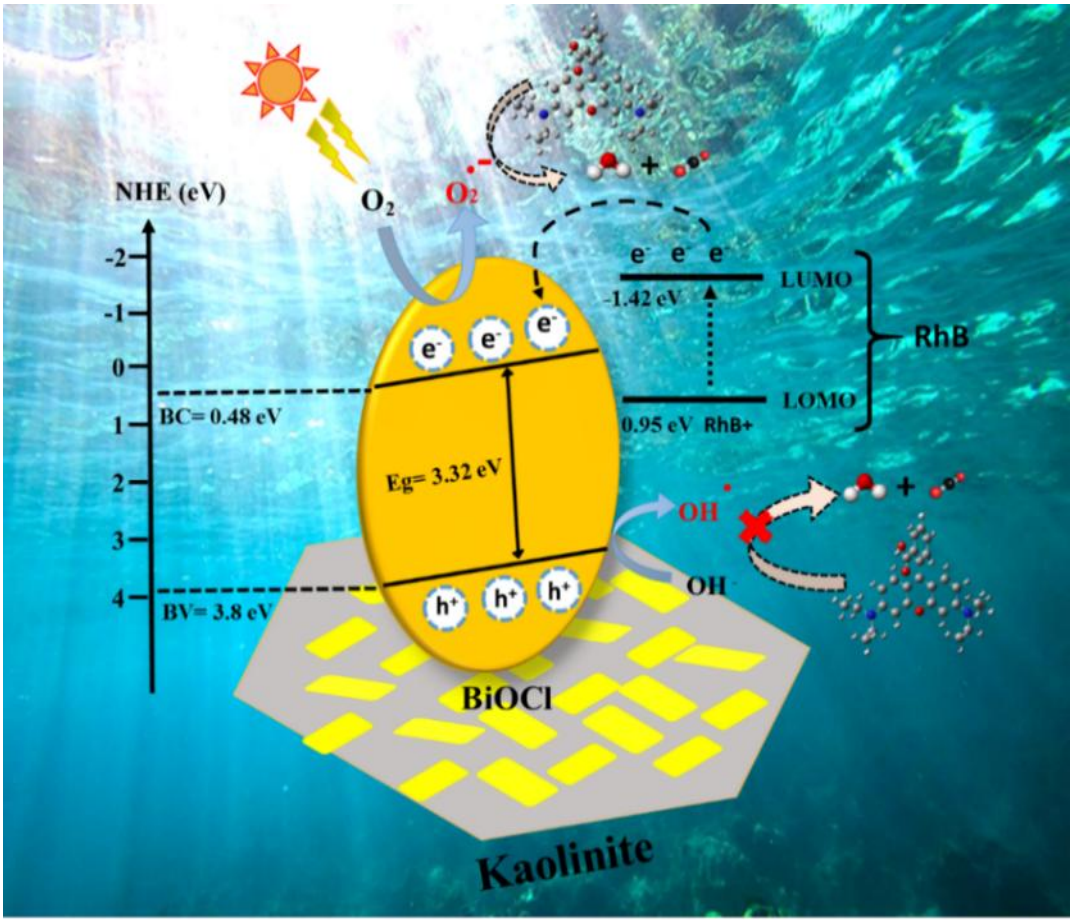

Fig. 16: The schematic mechanism of the photocatalytic performance of BiOCl@0.4Kaol.

3.9. Stability and recyclability

To evaluate the recyclability and the stability of BiOCl@Kaol photocatalyst, a test of regeneration was investigated. Firstly, the BiOCl@Kaol composite was used in the first time. After completely RhB dye degradation under sunlight irradiation, the BiOCl@Kaol was collected by centrifuge, washed three times by distilled water and ethanol, dried in the oven at 80 °C for 12 hours for a future use. This operation has been spotted 5 times. The experimental results represented in Fig. 17, showed that the degradation efficiency remains stable after 5 cycling runs, and the removal efficiency has been slightly reduced from 100% to 98.6 %, after 5 cycles, in comparison to pure BiOCl for which the photodegradation efficiency was reduced from 72% to 15 % after 5 cycles.

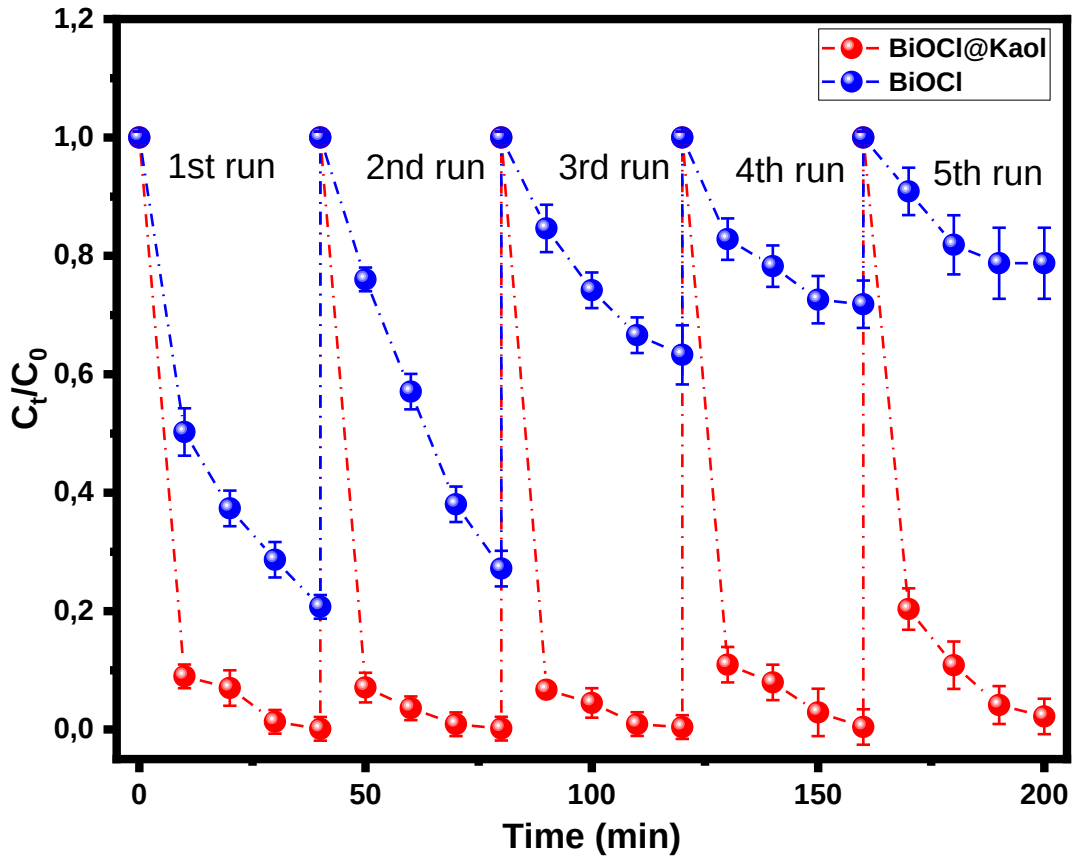

Fig. 17: Cycling runs of RhB dye photodegradation by BiOCl@0.4Kaol and by pure BiOCl.

In addition, the photodegradation efficiency of RhB dye by our synthetized nanocomposite was compared with other BiOCl modification in different literature (**Table. 4**). As can be seen from the table 4, the BiOCl@Kaol composite has a strongly performance in sunlight irradiation (100% after 35 min) compared with other composites, indicating the successful prepared nanocomposite.

Table. 4: Comparison of photodegradation of RhB dye using different BiOCl modification.

Photocatalyst	**Photocatalyst/ pollutant concentration**	**Light source**	**Photodegradation Efficiency**	**Reference**
2D/3D BiOCl/Bi_5O_7I	25 mg / 100 mL of 10 mg/L	UV light	97.7% in 70 min	[45]
Ag_2WO_4/ BiOCl	30 mg / 50 mL of 5 mg/L	UV light	81.3% in 25 min	[46]
WO_3/BiOCl	50 mg / 50 mL of 30 mg/L	Visible light	100% after 180 min	[47]
BiOCl/TiO_2–zeolite	100 mg / 100 mL of 10 mg/L	visible light	87.10 within 90 min	[32]
BiOCl@Kaol	100 mg / 100 mL of 10 mg/L	Sunlight	100% after 35 min	This work
Pure BiOCl	100 mg / 100 mL of 10 mg/L	Sunlight	71% after 40 min	This work

4. Conclusion

In conclusion, a series of BiOCl@Kaol composite photocatalysts, having various clay/BiOCl weight ratios, were prepared by using a simple one-step precipitation method in acidic medium. The synthesized BiOCl@Kaol hybrid photocatalyst materials were then characterized by several techniques such as XRD, SEM, EDX, TEM, and UV-vis DRS and finally applied for rapid removal of RhB dye from aqueous solution by photocatalytic reaction under sunlight irradiation. Thus, all the samples were found to be efficient for RhB degradation, and more than 100% of the dye was degraded within 35 min for an optimal clay/BiOCl weight ratio of 0.4 (BiOCl@0.4Kaol). Further, the synthetized photocatalysts were found to be stable after 5 cycling runs. The overall data indicate that the synthesis protocol and the application process as used in the present work, bring a lot of hope for large-scale applications. In addition, the DFT-D and MD simulations were used to elucidate the adsorption mechanisms of BiOCl on kaolinite particles, and RhB molecules on BiOCl@Kaol. Hence, based on the MD simulations and Monte Carlo calculations, it was found that the BiOCl molecules were approximately parallel to the kaolinite surfaces containing -OH groups, and one of the (001) kaolinite surfaces bearing OH groups formed hydrogen bonding with the BiOCl-O atoms materials. Moreover, the results demonstrated that the interactions occurring between RhB molecules and BiOCl@Kaol were Van der Waals type. Finally, the adsorption energies of BiOCl on kaolinite particles, and RhB molecules on BiOCl@Kaol, were found to be negative, indicating a stable and exothermic system.

Acknowledgements

This work results from a collaborative effort between involving scientific members of Faculté des Sciences d'Agadir, Faculté des Sciences Appliquées d'Ait Melloul, Université Ibn Zohr, Agadir-Morocco, and Institut de Sciences Des Matériaux De Mulhouse (IS2M-UMR 7361 CNRS), Université de Haute Alsace (UHA), Mulhouse-France. We thank VIDAL Loïc (IS2M-Mulhouse-France), VAULOT Cyril (IS2M-Mulhouse-France) and GREE Simon (IS2M-Mulhouse-France), for the Transmission electron microscopy (TEM), Ultraviolet–Visible Diffuse Reflectance Spectroscopy (UV–Vis DRS) and the Fourier-transform infrared spectroscopy (FT-IR) analyzes, respectively.

References

[1] H. Ouachtak, S. Akhouairi, R. Haounati, A.A. Addi, A. Jada, M.L. Taha, J. Douch, 3,4-dihydroxybenzoic acid removal from water by goethite modified natural sand column fixed-bed: Experimental study and mathematical modeling, Desalin. Water Treat. 194 (2020) 439–449. https://doi.org/10.5004/dwt.2020.25562.

[2] A. Regti, Z. Lakbaibi, H. Ben El Ayouchia, M. El Haddad, M.R. Laamari, M. El Himri, R. Haounati, Hybrid Methods Combining Computational and Experimental Measurements for the Uptake of Eriochrome Black T Dye Utilising Fish Scales, Int. J. Environ. Anal. Chem. (2021) 1–20. https://doi.org/10.1080/03067319.2021.1929199.

[3] H. Ouachtak, A. El Guerdaoui, R. Haounati, S. Akhouairi, R. El Haouti, N. Hafid, A. Ait Addi, B. Šljukić, D.M.F. Santos, M.L. Taha, Highly efficient and fast batch adsorption of orange G dye from polluted water using superb organo-montmorillonite: Experimental study and molecular dynamics investigation, J. Mol. Liq. 335 (2021) 116560. https://doi.org/10.1016/j.molliq.2021.116560.

[4] G. Zhu, M. Hojamberdiev, K.I. Katsumata, N. Matsushita, K. Okada, P. Liu, J. Zhou, Y. Liu, Synthesis of Heterostructured In2O3/BiOCl powders and their visible-light-driven photocatalytic activity for the degradation of Rhodamine B, Adv. Powder Technol. 25 (2014) 1292–1303. https://doi.org/10.1016/j.apt.2014.03.008.

[5] R. Haounati, F. Alakhras, H. Ouachtak, T.A. Saleh, G. Al-Mazaideh, E. Alhajri, A. Jada, N. Hafid, A.A. Addi, Synthesized of Zeolite@Ag2O Nanocomposite as Superb Stability Photocatalysis Toward Hazardous Rhodamine B Dye from Water, Arab. J. Sci. Eng. (2022). https://doi.org/10.1007/s13369-022-06899-y.

[6] T.A. Khan, S. Dahiya, I. Ali, Use of kaolinite as adsorbent : Equilibrium , dynamics and thermodynamic studies on the adsorption of Rhodamine B from aqueous solution, Appl. Clay Sci. 69 (2012) 58–66.

[7] A. Studies, M.A. Khan, M.R. Siddiqui, M. Otero, Removal of Rhodamine B from Water Using a Solvent Impregnated Polymeric Dowex 5WX8 Resin : Statistical Optimization and Batch, Polymers (Basel). (2020) 1–12.

[8] S. Zhang, L. Zhong, J. Wang, A. Tang, H. Yang, Porous carbon-based MgAlF5·1.5H2O composites derived from carbon- coated clay presenting super high adsorption capacity for Congo Red, Chem. Eng. J. 406 (2021) 126784. https://doi.org/10.1016/j.cej.2020.126784.

[9] A.P. Bhat, P.R. Gogate, Cavitation-based pre-treatment of wastewater and waste sludge for improvement in the performance of biological processes: A review, Biochem. Pharmacol. (2020) 104743. https://doi.org/10.1016/j.jece.2020.104743.

[10] R. Haounati, H. Ouachtak, R. El, S. Akhouairi, F. Largo, Elaboration and properties of a new SDS / CTAB @ Montmorillonite organoclay composite as a superb adsorbent for the removal of malachite green from aqueous solutions, Sep. Purif. Technol. 255 (2021) 117335. https://doi.org/10.1016/j.seppur.2020.117335.

[11] A. Imgharn, H. ighnih, A. Hsini, Y. Naciri, M. Laabd, H. Kabli, M. Elamine, R. Lakhmiri, B. Souhail, A. Albourine, Synthesis and characterization of polyaniline-based biocomposites and their application for effective removal of Orange G dye using adsorption in dynamic regime, Chem. Phys. Lett. 778 (2021) 138811. https://doi.org/10.1016/j.cplett.2021.138811.

[12] A. Yusaf, M. Usman, A. Mansha, M. Saeed, M. Ahmad, M. Siddiq, Micellar-enhanced ultrafiltration (MEUF) for removal of rhodamine B (RhB) from aqueous system, J. Dispers. Sci. Technol. 43 (2022) 366–348. https://doi.org/10.1080/01932691.2020.1841002.

[13] X. Liu, Z. Chen, W. Du, P. Liu, L. Zhang, F. Shi, Treatment of wastewater containing methyl orange dye by fluidized three dimensional electrochemical oxidation process integrated with chemical oxidation and adsorption, J. Environ. Manage. 311 (2022) 114775. https://doi.org/10.1016/j.jenvman.2022.114775.

[14] P. Tun, K. Wang, H. Naing, J. Wang, G. Zhang, Facile preparation of visible-light-responsive kaolin-supported Ag @ AgBr composites and their enhanced photocatalytic properties, Appl. Clay Sci. 175 (2019) 76–85. https://doi.org/10.1016/j.clay.2019.04.003.

[15] X. Ma, H. Cheng, Facet-dependent photocatalytic H2O2 production of single phase Ag3PO4 and Z-scheme Ag/ZnFe2O4-Ag-Ag3PO4 composites, Chem. Eng. J. 429 (2022) 132373. https://doi.org/10.1016/j.cej.2021.132373.

[16] O.A. Oyewo, A. Adeniyi, B.B. Sithole, M.S. Onyango, Sawdust-Based Cellulose Nanocrystals Incorporated with ZnO Nanoparticles as Efficient Adsorption Media in the Removal of Methylene Blue Dye, ACS Omega. 5 (2020) 18798–18807. https://doi.org/10.1021/acsomega.0c01924.

[17] M.E. Borges, M. Sierra, E. Cuevas, R.D. García, P. Esparza, Photocatalysis with solar energy: Sunlight-responsive photocatalyst based on TiO2 loaded on a natural material for wastewater treatment, Sol. Energy. 135 (2016) 527–535. https://doi.org/10.1016/j.solener.2016.06.022.

[18] E. Amaterz, A. Tara, A. Bouddouch, A. Taoufyq, B. Bakiz, F. Lazar, M. Gilliot, A. Benlhachemi, L. Bazzi, O. Jbara, Hierarchical flower-like SrHPO4 electrodes for the photoelectrochemical degradation of Rhodamine B, J. Appl. Electrochem. 50 (2020) 569–581. https://doi.org/10.1007/s10800-020-01416-1.

[19] G. Zhao, J. Zou, J. Hu, X. Long, F. Jiao, A critical review on graphitic carbon nitride (g-C 3 N 4) -based composites for environmental remediation, Sep. Purif. Technol. 279 (2021) 119769. https://doi.org/10.1016/j.seppur.2021.119769.

[20] J. Wang, H. Li, X. Yan, C. Qian, Y. Xing, S. Yang, Z. Kang, J. Han, W. Gu, H. Yang, F. Xiao, Synergistic enhancement of the visible-light photocatalytic activity of hierarchical 3D BiOClxBr1-x/graphene oxide heterojunctions for formaldehyde degradation at room temperature, J. Alloys Compd. 795 (2019) 120–133. https://doi.org/10.1016/j.jallcom.2019.04.176.

[21] Z. Xu, C. Zhang, Y. Zhang, Y. Gu, Y. An, BiOCl-based photocatalysts : Synthesis methods , structure , property , application , and perspective, Inorg. Chem. Commun. 138 (2022) 109277. https://doi.org/10.1016/j.inoche.2022.109277.

[22] F. Mokhtari, N. Tahmasebi, Hydrothermal synthesis of W-doped BiOCl nanoplates for photocatalytic degradation of rhodamine B under visible light, J. Phys. Chem. Solids. 149 (2021) 109804. https://doi.org/10.1016/j.jpcs.2020.109804.

[23] A. Kundu, S. Sharma, S. Basu, Modulated BiOCl nanoplates with porous g-C 3 N 4 nanosheets for photocatalytic degradation of color / colorless pollutants in natural sunlight, J. Phys. Chem. Solids. 154 (2021) 110064. https://doi.org/10.1016/j.jpcs.2021.110064.

[24] C. Cao, L. Xiao, C. Chen, Q. Cao, Applied Surface Science Synthesis of novel Cu 2 O / BiOCl heterojunction nanocomposites and their enhanced photocatalytic activity under visible light, 357 (2015) 1171–1179.

[25] J. Chang, Y. Zhong, C. Hu, J. Luo, P. Wang, Synthesis and signi fi cantly enhanced visible light photocatalytic activity of BiOCl / AgBr heterostructured composites, Inorg. Chem. Commun. 96 (2018) 145–152. https://doi.org/10.1016/j.inoche.2018.08.010.

[26] W. Liu, L. Qiao, A. Zhu, Y. Liu, J. Pan, Constructing 2D BiOCl / C 3 N 4 layered composite with large contact surface for visible-light-driven photocatalytic degradation, Appl. Surf. Sci. 426 (2017) 897–905. https://doi.org/10.1016/j.apsusc.2017.07.225.

[27] S. Adhikari, D. Kim, Influence of surfactant on the synthesis of BiOCl / WO 3 microcomposites for enhanced adsorption in aqueous solutions, Korean J. Chem. Eng. 35 (2018) 1–10. https://doi.org/10.1007/s11814-018-0167-9.

[28] H.H. Naing, Y. Li, J.B. Ghasemi, J. Wang, G. Zhang, Enhanced visible-light-driven photocatalysis of in-situ reduced of bismuth on BiOCl nanosheets and montmorillonite loading: Synergistic effect and mechanism insight, Chemosphere. 304 (2022) 135354. https://doi.org/10.1016/j.chemosphere.2022.135354.

[29] Z. Cao, Q. Wang, H. Cheng, Recent advances in kaolinite-based material for photocatalysts, Chinese Chem. Lett. (2021). https://doi.org/10.1016/j.cclet.2021.01.009.

[30] X. Hu, Z. Sun, J. Song, G. Zhang, C. Li, S. Zheng, Synthesis of novel ternary heterogeneous BiOCl/TiO2/sepiolite composite with enhanced visible-light-induced photocatalytic activity towards tetracycline, J. Colloid Interface Sci. 533 (2019) 238–250. https://doi.org/10.1016/j.jcis.2018.08.077.

[31] J. Luo, Y. Luo, J. Yao, M. Zhang, S. Chen, X. Liu, Composite microsphere resulting from assembly of BiOCl nanosheets and palygorskite nanorods for enhanced photocatalytic activity, Appl. Clay Sci. 168 (2019) 450–458. https://doi.org/10.1016/j.clay.2018.12.002.

[32] G. Zhang, Z. Sun, X. Hu, A. Song, S. Zheng, Synthesis of BiOCl/TiO2–zeolite composite with enhanced visible light photoactivity, J. Taiwan Inst. Chem. Eng. 81 (2017) 435–444. https://doi.org/10.1016/j.jtice.2017.09.030.

[33] Y. Zhao, Z. Cao, A.A. Zuh, Y. Jia, Q. Wang, H. Cheng, Synthesis of bismuth oxyiodide/kaolinite composite with enhanced photocatalytic activity, J. Phys. Chem. Solids. 161 (2022) 110424. https://doi.org/10.1016/j.jpcs.2021.110424.

[34] M. Hamdi Karaoğlu, M. Doğan, M. Alkan, Removal of cationic dyes by kaolinite, Microporous Mesoporous Mater. 122 (2009) 20–27. https://doi.org/10.1016/j.micromeso.2009.02.013.

[35] D. Jiang, Z. Liu, L. Fu, H. Yang, Interfacial Chemical-Bond-Modulated Charge Transfer of Heterostructures for Improving Photocatalytic Performance, ACS Appl. Mater. Interfaces. 12 (2020) 9872–9880. https://doi.org/10.1021/acsami.9b17183.

[36] X. Zhang, Y. Liu, C. Li, L. Tian, F. Yuan, S. Zheng, Z. Sun, Fast and lasting electron transfer between γ-FeOOH and g-C3N4/kaolinite containing N vacancies for enhanced visible-light-assisted peroxymonosulfate activation, Chem. Eng. J. 429 (2022) 132374. https://doi.org/10.1016/j.cej.2021.132374.

[37] B. Fahimirad, R.E. Malekshah, M.A. Chamjangali, R.K. Abasabadi, S. Bromand, Theoretical and experimental study of the photodegradation of methyl orange in the presence of different morphologies of Au-ZnO using Monte Carlo dynamic simulation, Environ. Sci. Pollut. Res. (2022). https://doi.org/10.1007/s11356-022-19657-2.

[38] B. Li, S. Liu, J. Guo, L. Zhang, Interaction between low rank coal and kaolinite particles: A DFT simulation, Appl. Surf. Sci. 456 (2018) 215–220. https://doi.org/10.1016/J.APSUSC.2018.06.121.

[39] R. Nematollahi, B. Fahimirad, R. Eshaghi Malekshah, A. Elhampour, M. Piri, M.M. Heravi, Experimental and theoretical studies on the synergistic effect of P and Se co-doped g-C3N4 loaded with Ag nanoparticles as an affective photocatalyst under visible light irradiation, J.

Mol. Liq. 369 (2023) 120387. https://doi.org/10.1016/J.MOLLIQ.2022.120387.

[40] Z. Yang, W. Liu, H. Zhang, X. Jiang, F. Min, DFT study of the adsorption of 3-chloro-2-hydroxypropyl trimethylammonium chloride on montmorillonite surfaces in solution, Appl. Surf. Sci. 436 (2018) 58–65. https://doi.org/10.1016/J.APSUSC.2017.12.011.

[41] L. Liu, F. Min, J. Chen, F. Lu, L. Shen, The adsorption of dodecylamine and oleic acid on kaolinite surfaces: Insights from DFT calculation and experimental investigation, Appl. Surf. Sci. 470 (2019) 27–35. https://doi.org/10.1016/J.APSUSC.2018.11.104.

[42] R. Haounati, A. El Guerdaoui, H. Ouachtak, R. El Haouti, A. Bouddouch, N. Hafid, B. Bakiz, D.M.F. Santos, M. Labd Taha, A. Jada, A. Ait Addi, Design of direct Z-scheme superb magnetic nanocomposite photocatalyst Fe3O4/Ag3PO4@Sep for hazardous dye degradation, Sep. Purif. Technol. 277 (2021) 119399. https://doi.org/10.1016/j.seppur.2021.119399.

[43] M. Chakraborty, K.K. Bera, S. Chatterjee, A. Ghosh, S.K. Bhattacharya, Synthesis of mesoporous BiOI flower and facile in-situ preparation of BiOI/BiOCl mixture for enhanced photocatalytic degradation of toxic dye, Rhodamine-B, J. Photochem. Photobiol. 8 (2021) 100077. https://doi.org/10.1016/j.jpap.2021.100077.

[44] J. Wang, Z. Zhang, Co-precipitation synthesis and photocatalytic properties of BiOCl micro fl owers, Opt. - Int. J. Light Electron Opt. 204 (2020) 164149. https://doi.org/10.1016/j.ijleo.2019.164149.

[45] W. Huang, X. Xiao, M. Lu, Y. Xiao, In-situ fabrication of novel BiOCl/Bi5O7I 2D/3D heterostructures with enhanced photocatalytic activity, J. Alloys Compd. 895 (2022) 162669. https://doi.org/10.1016/j.jallcom.2021.162669.

[46] S. Cen, X. Lv, Q. Liu, D. Li, Y. Jiang, C. Hou, P. Zhang, Y. Xu, Direct Z-scheme Ag2WO4/BiOCl composite photocatalyst for efficient photocatalytic degradations of dissolved organic impurities, Optik (Stuttg). 243 (2021) 166847. https://doi.org/10.1016/j.ijleo.2021.166847.

[47] S. Shamaila, A.K.L. Sajjad, F. Chen, J. Zhang, WO3/BiOCl, a novel heterojunction as visible light photocatalyst, J. Colloid Interface Sci. 356 (2011) 465–472. https://doi.org/10.1016/j.jcis.2011.01.015.